

Activation of the Rab7 GTPase by the MON1-CCZ1 Complex Is Essential for PVC-to-Vacuole Trafficking and Plant Growth in *Arabidopsis*^{CJW}

Yong Cui,^a Qiong Zhao,^a Caiji Gao,^a Yu Ding,^a Yonglun Zeng,^a Takashi Ueda,^b Akihiko Nakano,^b and Liwen Jiang^{a,c,1}

^aSchool of Life Sciences, Centre for Cell and Developmental Biology and State Key Laboratory of Agrobiotechnology, The Chinese University of Hong Kong, Shatin, New Territories, Hong Kong, China

^bDepartment of Biological Sciences, Graduate School of Science, University of Tokyo, Bunkyo-ku, Tokyo 113-0033, Japan

^cShenzhen Research Institute, The Chinese University of Hong Kong, Shenzhen 518057, China

ORCID ID: 0000-0002-8861-8416 (Y.C.)

Rab GTPases serve as multifaceted organizers during vesicle trafficking. Rab7, a member of the Rab GTPase family, has been shown to perform various essential functions in endosome trafficking and in endosome-to-lysosome trafficking in mammalian systems. The *Arabidopsis thaliana* genome encodes eight putative Rab7 homologs; however, the detailed function and activation mechanism of Rab7 in plants remain unknown. Here, we demonstrate that *Arabidopsis* RABG3f, a member of the plant Rab7 small GTPase family, localizes to prevacuolar compartments (PVCs) and the tonoplast. The proper activation of Rab7 is essential for both PVC-to-vacuole trafficking and vacuole biogenesis. Expression of a dominant-negative Rab7 mutant (RABG3f^{T22N}) induces the formation of enlarged PVCs and affects vacuole morphology in plant cells. We also identify *Arabidopsis* MON1 (MONENSIN SENSITIVITY1) and CCZ1 (CALCIUM CAFFEINE ZINC SENSITIVITY1) proteins as a dimeric complex that functions as the Rab7 guanine nucleotide exchange factor. The MON1-CCZ1 complex also serves as the Rab5 effector to mediate Rab5-to-Rab7 conversion on PVCs. Loss of functional MON1 causes the formation of enlarged Rab5-positive PVCs that are separated from Rab7-positive endosomes. Similar to the dominant-negative Rab7 mutant, the *mon1* mutants show pleiotropic growth defects, fragmented vacuoles, and altered vacuolar trafficking. Thus, Rab7 activation by the MON1-CCZ1 complex is critical for vacuolar trafficking, vacuole biogenesis, and plant growth.

INTRODUCTION

In plant cells, there are two different endomembrane trafficking pathways that play crucial roles in trafficking of vacuolar cargo proteins: the secretory pathway and the endocytic pathway (Jiang and Rogers, 1999; Nielsen et al., 2008). For the secretory pathway, proteins are synthesized in the endoplasmic reticulum (ER). Properly folded proteins with the appropriate targeting signals are subsequently transported to the Golgi apparatus (Jiang and Rogers, 1998; Vitale and Raikhel, 1999; Kincaid and Cooper, 2007). According to the classical model for vacuolar protein sorting, vacuolar proteins are recognized by vacuolar sorting receptors (VSRs) at the *trans*-Golgi network (TGN) and packaged into clathrin-coated vesicles (Kirsch et al., 1994). In the classical model, proteins with vacuolar sorting determinants are recruited by VSR proteins and delivered to the PVCs (Jiang and Rogers, 1998; daSilva et al., 2006; Mo et al., 2006), while those without targeting signals are secreted to the plasma membrane (PM) through default pathways (Jiang and Sun, 2002; Belenkaya et al., 2008; Collette et al., 2009; Toyooka et al., 2009). Due to low pH in

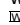
PVCs, cargo proteins delivered to PVCs were thought to dissociate from receptors and then be sent to vacuoles while the VSRs recycled back to Golgi or the TGN via a retromer complex (Lam et al., 2007b; Shen et al., 2013b). Recently, this classical view has been challenged, and the new model emphasizes the role of calcium in addition to pH (Robinson and Pimpl, 2014). In this model, VSRs interact with vacuolar cargo ligands already in the ER and retromers recycle VSRs from the TGN to the ER (Niemes et al., 2010; Robinson et al., 2012). In particular, the exact location and mechanism of retromer-mediated VSR recycling still remain unclear. On the other hand, for the endocytic pathway, proteins are internalized at the PM and reach vacuoles via several intermediate endosomal compartments, including TGNs/early endosomes and PVCs/late endosomes, where the early endosomes also serve as recycling endosomes for the recycling of proteins back to PM (Hwang and Robinson, 2009; Zouhar et al., 2009; Viotti et al., 2010). Secretory and endocytic pathways merge in the TGN in plant cells (Dettmer et al., 2006; Lam et al., 2007c; Chow et al., 2008; Viotti et al., 2010). PVCs may be derived from TGNs and fuse with vacuoles (Scheuring et al., 2011); however, the underlying mechanism of PVC maturation remains unknown.

In endomembrane trafficking system, the efficient and accurate fusion of membranes is an important requirement for protein trafficking in cells (Bottanelli et al., 2011). The specificity of vesicular transport relies mainly on the Rab GTPases, which coordinate membrane traffic and function as molecular switches (Stenmark, 2009). The inactive (GDP-bound) form of Rab requires a guanine nucleotide exchange factor (GEF) for its conversion to

¹ Address correspondence to ljiang@cuhk.edu.hk.

The author responsible for distribution of materials integral to the findings presented in this article in accordance with the policy described in the Instructions for Authors (www.plantcell.org) is: Liwen Jiang (ljiang@cuhk.edu.hk).

 Some figures in this article are displayed in color online but in black and white in the print edition.

 Online version contains Web-only data.

www.plantcell.org/cgi/doi/10.1105/tpc.114.123141

the active (GTP-bound) form. Then, effectors such as tethering factors and SNAREs (soluble *N*-ethylmaleimide-sensitive factor attachment protein receptors) are recruited to the GTP-bound Rab to promote membrane fusion (Novick et al., 2006; Cai et al., 2007; Markgraf et al., 2007; Nielsen et al., 2008; Qiu, 2012).

In plant cells, Rab7 proteins are thought to be localized to the tonoplast, which mediates the final step of vacuolar trafficking (Nahm et al., 2003; Mazel et al., 2004; Limpens et al., 2009; Rho et al., 2009; Heo et al., 2010; Kwon et al., 2010). However, details of Rab7 function in PVC-to-vacuole trafficking are still unknown (Nielsen et al., 2008). Recent studies in yeast and animal cells reveal that the dimeric MON1-CCZ1 complex is the Rab7 GEF mediating a Rab5-to-Rab7 conversion, in which the early endosome-localized Rab5 is replaced by Rab7, resulting in a Rab7-positive late endosome (Poteryaev et al., 2007, 2010; Kinchen and Ravichandran, 2010; Nordmann et al., 2010). However, in plant cells, the molecular mechanism underlying Rab7 activation and whether a comparable Rab5-to-Rab7 cascade exists are still unknown (Scheuring et al., 2011). The aim of this study is to use Rab7 and *Arabidopsis thaliana* MONENSIN SENSITIVITY1 (MON1) and CALCIUM CAFFEINE ZINC SENSITIVITY1 (CCZ1) homolog proteins as probes to investigate the plant vacuolar trafficking from the PVC to the vacuole using a combination of live-cell imaging, biochemical, and genetic approaches.

The *Arabidopsis* genome encodes eight putative Rab7 proteins (Vernoud et al., 2003). Multiple combinations of different Rab7 T-DNA insertion mutations lead to no obvious phenotype, suggesting that the functions of Rab7 proteins are highly redundant (Nielsen et al., 2008). Since *RABG3f* is highly expressed in different tissues and development stages of *Arabidopsis* (<http://www.geneinvestigator.ethz.ch>) (Zimmermann et al., 2004), we choose *RABG3f* as a representative to investigate Rab7 function and activation in *Arabidopsis*.

In this study, we demonstrated that (1) proper activation of Rab7 is essential for its localization and function; (2) expression of a dominant-negative Rab7 mutant induces the formation of enlarged PVCs, affects vacuole morphology, inhibits vacuolar trafficking, and causes seedling death; (3) the MON1-CCZ1 complex preferentially binds to inactive Rab7 and functions as a Rab7 GEF; (4) through direct interaction with active Rab5, the MON1-CCZ1 complex also serves as the Rab5 effector, thus linking activated Rab5 to Rab7 recruitment in plants; (5) without functional MON1, Rab5-positive endosomes are separate from Rab7-positive ones, supporting the bridging role of the MON1-CCZ1 complex in Rab5-to-Rab7 conversion; and (6) similar to the dominant-negative *Rab7* mutant, the *mon1* mutant also contains enlarged PVCs and fragmented vacuoles, exhibits defects in vacuolar trafficking, and shows retarded growth. Taken together, these results demonstrate that MON1-CCZ1 complex-mediated Rab7 activation is critical for vacuolar trafficking and plant growth.

RESULTS

RABG3f (Rab7) Localizes to PVCs and the Tonoplast in *Arabidopsis* Cells

In order to study Rab7 function in PVC-to-vacuole trafficking, we first investigated the subcellular localization of active and

inactive forms of RABG3f in plant cells (Supplemental Figure 1). As shown in Figure 1A, dexamethasone (Dex)-induced expression of wild-type green fluorescent protein (GFP)-RABG3f showed endosome and tonoplast localization patterns. Constitutively active RABG3f (GFP-RABG3f^{Q67L}) showed mainly the tonoplast pattern, while dominant-negative RABG3f (GFP-RABG3f^{T22N}) showed a cytosolic and endosomal localization. This indicated that the inactive RABG3f was capable of being targeted to endosomes but failed to reach the tonoplast.

To identify RABG3f-localized endosomes, we compared the subcellular localization of RABG3f with different organelle markers via stable expression in transgenic *Arabidopsis* plants. As shown in Supplemental Figures 2A and 2B online, a *UBQ10* promoter-driven yellow fluorescent protein (YFP)-RABG3f fusion mainly showed the endosome and tonoplast localization patterns in *Arabidopsis* root and leaf cells, similar to the Dex-induced expression of GFP-RABG3f. The tonoplast-localized YFP-RABG3f colocalized with the tonoplast marker mCherry-VAMP711 (Ch-VAMP711), while YFP-RABG3f-positive endosomes were distinct from Ch-VAMP711-positive small vacuoles (Supplemental Figure 2C). When compared with the PVC marker line Ch-RHA1, 82% of the YFP-RABG3f-positive endosomes colocalized with 68% of the Ch-RHA1-positive PVCs (Figure 1B), suggesting that, besides tonoplast localization, RABG3f also localized to PVCs. Upon treatment with wortmannin (Wort), a specific inhibitor of phosphatidylinositol 3-kinase, YFP-RABG3f colocalized with Ch-RHA1 in enlarged endosomes or PVCs, seen as ring-like structures in a single optical confocal image (Supplemental Figure 2D), which further confirmed the PVC localization of RABG3f. In addition, 4D (3D image plus time) movie analysis of their dynamic relationship showed that YFP-RABG3f was gradually recruited to RHA1-positive PVCs (Supplemental Movie 1 and Supplemental Figure 3). The dual localizations of RABG3f to PVCs and the tonoplast suggest that it functions in mediating PVC-to-vacuole trafficking in plants.

Dominant-Negative Rab7 Induces the Formation of Enlarged PVCs, Affects Vacuole Morphology, and Inhibits Vacuolar Trafficking

Since Rab7 family proteins are highly redundant, in order to study Rab7 function in vacuolar trafficking, we used another strategy by exploiting *Arabidopsis* lines expressing a dominant-negative Rab7, RABG3f^{T22N} (Supplemental Figure 1). Expression of RABG3f^{T22N} induced 78% of YFP-ARA7 (PVC) and 65% of GFP-VSR1 (PVC) to form enlarged endosomes or PVCs in plant leaf and root cells, respectively (Figure 1C; Supplemental Figure 4A). In addition, abnormal or fragmented vacuoles were observed in plant leaf and root cells when expression of RABG3f^{T22N} was induced (Figure 1D), which showed that expression of RABG3f^{T22N} affected vacuole morphology. However, the expression of RABG3f^{T22N} did not significantly affect other organelle markers, including the TGN marker VHA1-GFP, the recycling endosome marker YFP-RABA1e, the Golgi marker YFP-SYP32, or the PM marker GFP-LTI6a (Supplemental Figures 4B to 4E). These results suggested that proper Rab7 activation was important for PVC and vacuole morphology.

To determine the membrane source of these RABG3f^{T22N}-induced enlarged structures, RABG3f^{T22N} was transiently expressed

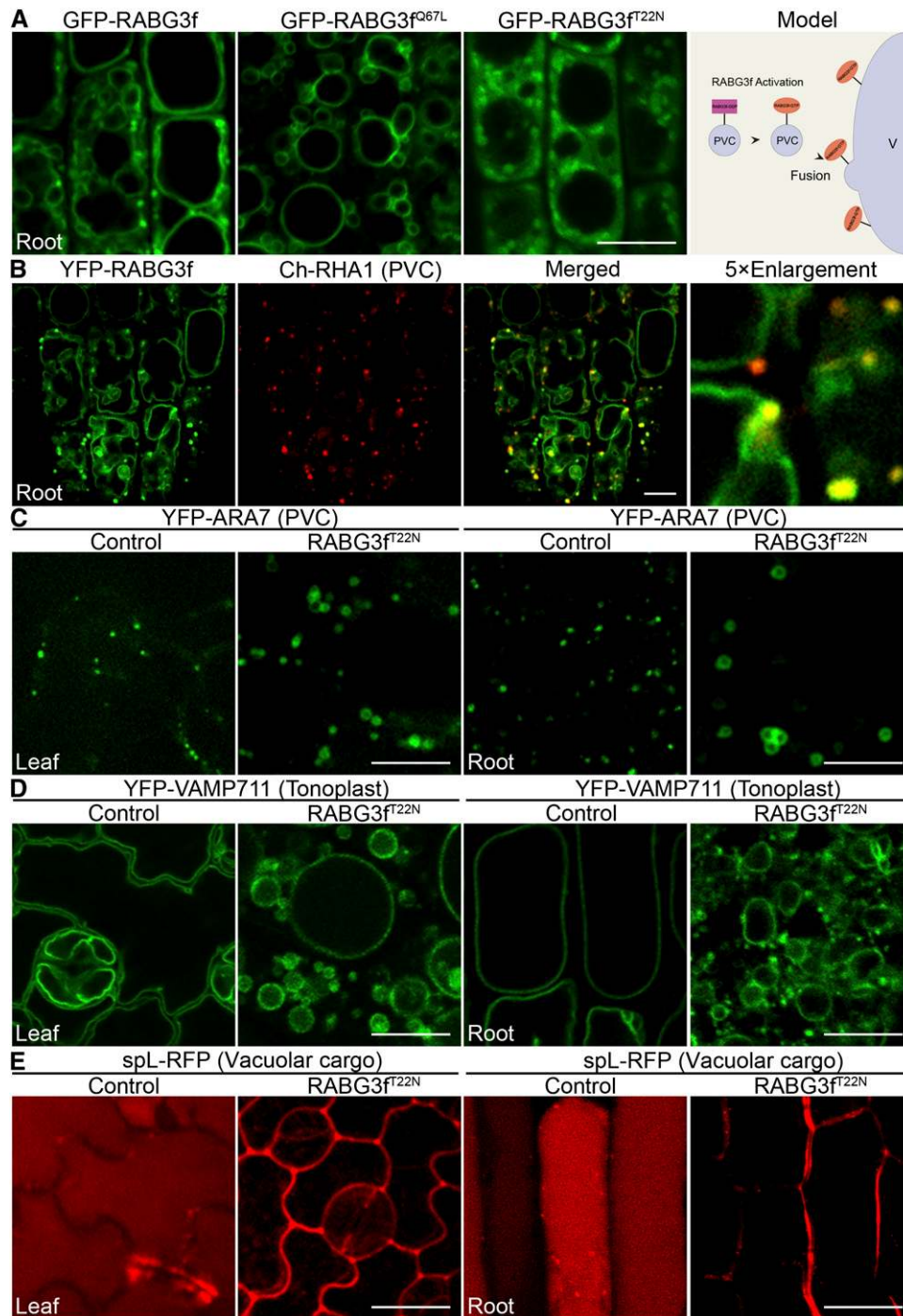


Figure 1. A Dominant-Negative RABG3f Mutant Protein Induces the Formation of Enlarged PVCs, Affects Vacuole Morphology, and Inhibits Vacuolar Trafficking.

(A) Subcellular localization of GFP-RABG3f, GFP-RABG3f^{Q67L}, and GFP-RABG3f^{T22N} expressed under a Dex-inducible promoter and working model of RABG3f localization in plant cells.

(B) YFP-RABG3f was crossed into a PVC marker line to analyze its localization.

(C) to (E) Confocal microscopy images of the PVC marker YFP-ARA7 **(C)**, the tonoplast marker YFP-VAMP711 **(D)**, and the lytic vacuolar cargo marker spL-RFP **(E)** in 6-d-old RABG3f^{T22N} seedlings grown in the absence or presence of 10 μ M Dex.

Bars = 10 μ m in **(A)** to **(E)**.

with different known organelle markers. Upon transient expression, RABG3f^{T22N} also induced YFP-ARA7 to form enlarged structures that were largely separate from the ER marker monomeric red fluorescent protein (mRFP)-HDEL, the Golgi marker ManI-mRFP, and the TGN marker mRFP-SYP61 (Supplemental Figures 5A to 5C). However, these YFP-ARA7-positive enlarged structures were mostly colocalized with the PVC marker mRFP-VSR2 (Supplemental Figure 5D). These results showed that the RABG3f^{T22N}-induced enlarged structures were PVCs in nature likely derived from homotypic PVC fusion.

In addition, RABG3f^{T22N} also inhibited vacuolar trafficking, since the soluble lytic vacuolar cargo marker spL-RFP was not delivered to vacuoles due to expression of RABG3f^{T22N} (Figure 1E). spL-RFP is an RFP fusion containing signal peptide (sp) and the sequence-specific vacuolar sorting signals (ssVSS) of proclin. This fusion protein is transported to lytic vacuole when expressed in plant cells (Hunter et al., 2007). Indeed, similar secretion phenomena of mis-sorted vacuolar cargoes have been shown in several vacuolar sorting mutants, for example, the *vps9a-2* mutant (loss-of-function mutant of Rab5 GEF) (Ebine et al., 2011) and the *vamp727 syp22* double mutant (a loss-of-function mutant of a SNARE complex) (Ebine et al., 2008). Similarly, expression of RABG3f^{T22N} may inhibit PVC fusion with vacuole, thus causing abnormal vacuolar trafficking and secretion of spL-RFP. The above results showed that the dominant-negative RABG3f^{T22N} induced the formation of enlarged PVCs, affected vacuole morphology, and inhibited vacuolar trafficking.

The Dominant-Negative Rab7 Inhibits Degradation of Storage Proteins in the Protein Storage Vacuole and Results in Seedling Death

Plants expressing dominant-negative Rab7 exhibited significant plant growth defects. As shown in Figure 2A, *Arabidopsis* seedlings expressing RABG3f^{T22N} (Line #3) died as seedlings, whereas wild-type seedlings and seedlings expressing the wild-type RABG3f appeared similar to each other. Two other lines, Line #8 and Line #12, showed weak and comparable phenotype compared with Line #3 (Supplemental Figure 6A). Consistent with the severity of their phenotypes, immunoblot analysis showed that the expression of Myc-RABG3f^{T22N} in Line #12 was higher than that in Line #8 (Supplemental Figure 6B). Moreover, the defective phenotypes of Line #3 were also exhibited in a Dex dose-dependent manner, indicating that these phenotypes were most likely caused by the expression of RABG3f^{T22N} (Supplemental Figure 6C). Statistical analysis of root lengths showed that expression of RABG3f^{T22N} resulted in significantly shorter roots versus wild-type or RABG3f seedlings (Figure 2B). Further control immunoblot experiments showed that the expression levels of RABG3f and RABG3f^{T22N} in transgenic plants were comparable (Figure 2C).

Furthermore, we analyzed the vacuolar trafficking of newly synthesized proteases in RABG3f^{T22N} Line #3 (hereafter designated simply RABG3f^{T22N}). Using protein extraction from seeds and seedlings of RABG3f^{T22N} grown in the absence or presence of 10 μ M Dex at 0 to 6 d after germination, the precursor of the protease aleurain was detected when RABG3f^{T22N} was induced (Figure 2D). Aleurain is a plant vacuolar thiol protease that is synthesized in the ER and transported to vacuoles via PVC and

processed into its mature form (Holwerda et al., 1992). Defects in vacuolar transport cause the secretion of aleurain in its precursor form (Shimada et al., 2003). Here, we detected accumulation of the precursor form of aleurain in plants expressing RABG3f^{T22N}. Such accumulation of aleurain precursor is likely due to its secretion into the extracellular space because RABG3f^{T22N} inhibited vacuolar trafficking. Interestingly, the mature form of aleurain in cells expressing Myc-RABG3f^{T22N} was similar to that in the wild-type cells, likely owing to unsuccessful vacuolar transport of mature aleurain.

Processing of aleurain from its precursor to mature form occurs in post-Golgi compartments (PVCs and vacuoles), while the degradation of storage proteins likely occurs in vacuoles (Rogers et al., 1997). In Myc-RABG3f^{T22N} plants, PVC to vacuolar trafficking was inhibited (Figure 1E). The vacuolar degradation of two native storage proteins, 12S globulin and 2S albumin, was also tested. In seeds and seedlings with induced expression of RABG3f^{T22N}, degradation of both storage proteins was largely delayed versus the control seeds/seedlings (Figure 2D), which was likely caused by the inhibition of vacuolar transport of the newly synthesized proteases upon RABG3f^{T22N} expression.

We also detected the protein storage vacuole (PSV) degradation process by observing PSV autofluorescence and the PSV marker line GFP-CT24. PSV autofluorescence signals in the cotyledons of RABG3f^{T22N} plants were still detectable at 3 d, and even at 6 d after germination (Supplemental Figures 7A to 7F). In comparison to the wild type, RABG3f^{T22N} plants showed significantly delayed storage protein degradation. Similarly, delayed degradation of GFP-CT24 was also detected when expression of RABG3f^{T22N} was induced, as evidenced by confocal microscopy images and immunoblot analysis of cotyledons 3 d after germination (Figures 2E and 2F). These results showed that expression of RABG3f^{T22N} delayed the degradation of storage proteins in the PSV during seed germination.

Next, as another control, we tested whether the addition of a nitrogen source to the medium would recover the lethal phenotype of RABG3f^{T22N}. We sprayed seeds on plates with 60 mM nitrogen. The lethal phenotype of RABG3f^{T22N} was slightly rescued, as the cotyledons became green when the seeds were germinated in medium containing 60 mM nitrogen (Supplemental Figures 7G to 7J). These results indicated that seedling death caused by expression of RABG3f^{T22N} was at least partially due to nitrogen nutrient mobilization defects. Taken together, RABG3f^{T22N} expression resulted in a lethal phenotype and also inhibited the trafficking of newly synthesized protease to vacuoles, thus leading to a delay in the degradation of storage proteins.

MON1 and CCZ1 Serve as a Rab7 GEF Complex That Preferentially Binds Inactive Rab7 on PVCs

Since the dominant-negative Rab7 inhibited PVC-to-vacuole trafficking and affected vacuole biogenesis, we suspected that a mutation in its GEF protein(s) would cause similar defects. However, in plant cells, Rab7 GEF proteins have not been identified as yet. Recent articles on yeast have reported that the MON1-CCZ1 complex serves as the Rab7 GEF (Nordmann et al., 2010). In *Arabidopsis*, there is one MON1 homolog (MON1, AT2G28390) and two CCZ1 homologs (CCZ1a, AT1G16020; CCZ1b, AT1G80910)

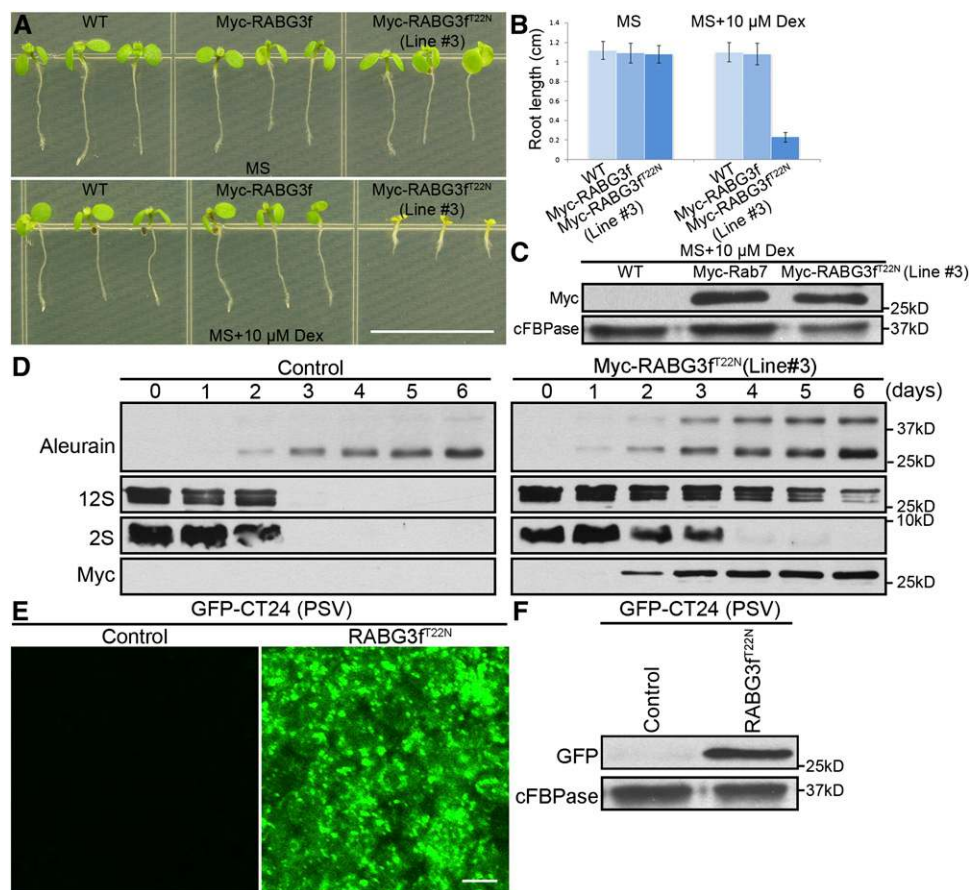


Figure 2. The Dominant-Negative RABG3f Mutant Protein Affects Degradation of Storage Proteins in the PSV and Results in Seedling Death.

(A) Phenotypes of 6-d-old seedlings of the wild type, Myc-RABG3f, and Myc-RABG3f^{T22N} (Line #3) grown in the absence or presence of 10 μ M Dex. (B) Root length of 6-d-old seedlings as indicated. Each column represents the mean of 30 seedlings. Error bars indicate sd.

(C) Immunoblot with Myc antibody from protein extracts of 6-d-old seedlings of the wild type, Myc-RABG3f, and Myc-RABG3f^{T22N} (Line #3) in the presence of 10 μ M Dex.

(D) Immunoblot analysis of seeds and seedlings of the RABG3f^{T22N} in the absence or presence of 10 μ M Dex at 0 to 6 d after germination with antibodies against Aleurain, 12S globulin, 2S albumin, and Myc. Aleurain precursor was detected in seedlings of the RABG3f^{T22N} in presence of 10 μ M Dex, suggesting that expression of RABG3f^{T22N} inhibited the transport of newly synthesized proteases to the vacuole.

(E) and (F) Confocal microscopy images and immunoblot analysis of the PSV marker GFP-CT24 in 3-d-old RABG3f^{T22N} seedlings grown in the absence or presence of 10 μ M Dex.

Bars = 1 cm in (A) and 10 μ m in (E).

[See online article for color version of this figure.]

(Supplemental Figures 8A and 8B). Specific MON1 antibodies were raised to test whether MON1 interacted with inactive Rab7 (Supplemental Figure 9A). Myc antibody-conjugated agarose beads were used to perform the immunoprecipitation of Myc-RABG3f^{T22N} protein in Myc-RABG3f^{T22N} plants. As shown in Supplemental Figure 9B, MON1 immunoprecipitated with inactive RABG3f in transgenic plants expressing Myc-RABG3f^{T22N}, suggesting that MON1 may activate RABG3f in plants.

To test whether MON1 and CCZ1 also served as a complex to activate RABG3f in *Arabidopsis*, we first analyzed the interaction between MON1 and CCZ1 via yeast two-hybrid (Y2H) and coimmunoprecipitation (Co-IP) assays. As shown in Figure 3A, MON1 and CCZ1 interacted with each other in Y2H assays. Co-IP experiments were also performed after transient coexpression of

YFP or YFP-CCZ1a with Myc-MON1 in *Arabidopsis* protoplasts. As shown in Figure 3B, Myc-MON1 specifically bound the YFP-CCZ1a and not YFP alone, suggesting that MON1 and CCZ1 interact and function as a complex.

To test if MON1-CCZ1 complex could activate Rab7 in *Arabidopsis*, we measured the *in vitro* GEF activity of MON1-CCZ1 complex toward Rab7 by monitoring the change in intrinsic tryptophan fluorescence upon nucleotide exchange (Pan et al., 1995; Antony et al., 2001; Goh et al., 2007). Since neither MON1 nor CCZ1 alone functions as the Rab7 GEF in yeast (Nordmann et al., 2010), we coexpressed MON1 and CCZ1 proteins to perform the *in vitro* GEF assay (Supplemental Figure 10). As shown in Figures 3C and 3D, MON1-CCZ1 complex stimulated the nucleotide exchange of RABG3f (Rab7) in a dose-dependent manner,

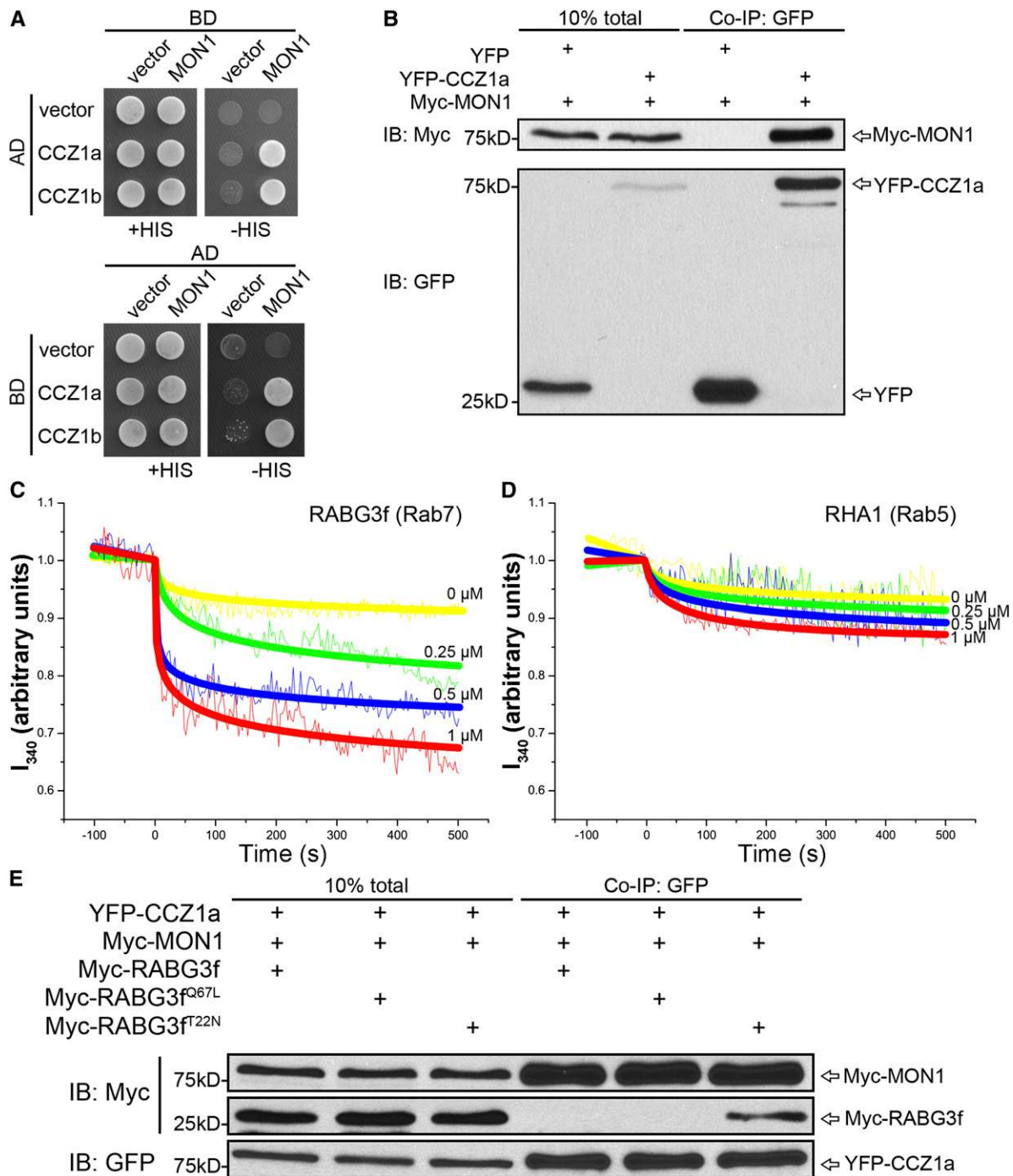


Figure 3. The MON1-CCZ1 Complex Serves as the Rab7 GEF in *Arabidopsis*.

(A) Y2H analysis of the interaction between MON1 and CCZ1. MON1, CCZ1a, and CCZ1b were used as either bait or prey. Interactions between two proteins were tested using the HIS3 reporter gene. AD, activation domain; BD, binding domain.

(B) Co-IP assays were performed after transient coexpression of YFP or YFP-CCZ1a with Myc-MON1 in *Arabidopsis* protoplasts. Total proteins (input) were subjected to immunoprecipitation with GFP-Trap beads followed by immunoblot analysis.

(C) and **(D)** In vitro GEF assay of MON1-CCZ1 complex. Nucleotide exchange on RABG3f (Rab7) **(C)** and RHA1 (Rab5) **(D)** was measured by monitoring tryptophan autofluorescence in the absence (yellow) or presence of 0.25 μ M (green), 0.5 μ M (blue), or 1 μ M (red) GST-CCZ1a-12 \times His-MON1. The jagged lines represent the raw data, and the bold lines represent the trend lines.

(E) Co-IP assays were performed after transient coexpression of YFP-CCZ1a, Myc-MON1 with wild-type, active, or inactive RABG3f in *Arabidopsis* protoplasts. Total proteins (input) were subjected to immunoprecipitation with GFP-Trap beads followed by immunoblot analysis.

while this complex showed limited GEF activity for RHA1 (Rab5). In addition, in protoplasts, this MON1-CCZ1 complex preferentially bound to inactive RABG3f (Figure 3E).

Theoretically, wild-type RABG3f should contain a GDP-bound form that can be recruited by the MON1-CCZ1 complex. However, as shown in Figure 3E, very little wild type form Myc-Rab7 was coimmunoprecipitated with the CCZ1 bait, which could be due to the possible transient interaction between wild-type Rab7 and the MON1-CCZ1 complex, as well as the relatively low efficiency of the Co-IP detection system. In addition, neither MON1 nor CCZ1a alone bound to any form of RABG3f (Supplemental Figure 11). These results indicated that MON1 and CCZ1 served as a GEF complex to activate Rab7 in *Arabidopsis*.

To determine where (at which organelle) MON1 and CCZ1 perform their function, GFP-MON1 and YFP-CCZ1a were transiently expressed in protoplasts for localization studies. As shown in Supplemental Figures 12A to 12F online, both GFP-MON1 and YFP-CCZ1a were found to be gradually recruited to endosomes

when they were expressed individually in protoplasts. As a control, GFP alone showed no recruitment even with a longer incubation time (Supplemental Figures 12G to 12I). MON1 and CCZ1 were recruited to the enlarged endosomes when coexpressed together with RABG3f^{T22N} or CFP-RABG3f^{T22N} (Figures 4A and 4B; Supplemental Figure 13A). To further identify these endosomes, we coexpressed RABG3f^{T22N}, XFP-MON1, and CCZ1a together with TGN or PVC markers. These results showed that these enlarged endosomes were enlarged PVCs (Figure 4C), but not TGN (Figure 4D). Compared with the RABG3f^{Q67L}, wild-type RABG3f was able to recruit mRFP-MON1 to endosomes, when coexpressed with CCZ1a (Supplemental Figures 13B and 13C). Similar to the Co-IP data, neither MON1 nor CCZ1 was recruited to the enlarged endosomes when individually coexpressed with RABG3f^{T22N} (Supplemental Figures 13D and 13E). These results show that the MON1-CCZ1 complex was recruited to PVCs first and then activated Rab7, which then mediated PVC-to-vacuole trafficking.

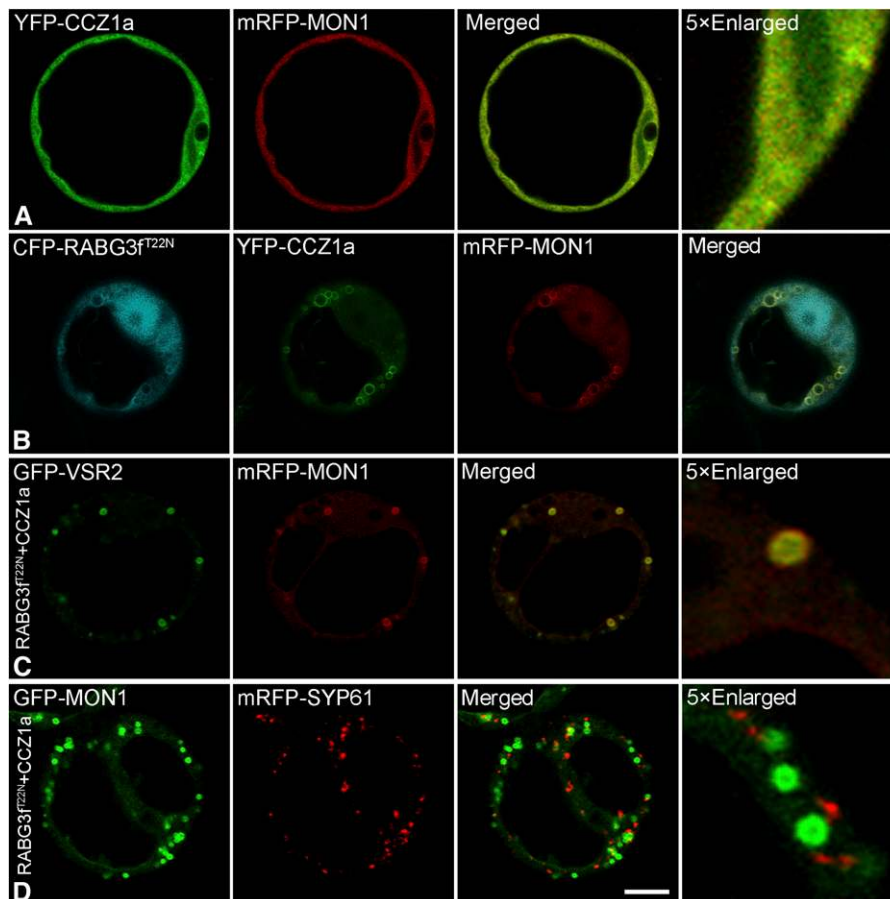


Figure 4. Subcellular Localization of MON1 and CCZ1 in *Arabidopsis* Protoplasts.

(A) Subcellular localization of mRFP-MON1 and YFP-CCZ1a in *Arabidopsis* protoplasts.

(B) mRFP-MON1 and YFP-CCZ1a were recruited to enlarged structures when coexpressed with CFP-RABG3f^{T22N}.

(C) and **(D)** RABG3f^{T22N}-induced, XFP-MON1-localized enlarged endosomes colocalized with PVC marker GFP-VSR2 but were separate from the TGN marker mRFP-SYP61.

Confocal images were collected from cells at 12 to 14 h after transfection. Bars = 10 μ m.

The MON1-CCZ1 Complex Is the Rab5 Effector and Is Recruited to PVCs by Active Rab5

In yeast cells, the MON1-CCZ1 complex is recruited to the membrane by active Rab5 protein (Nordmann et al., 2010). Whether a similar recruitment of MON1-CCZ1 complex exists in plants is a matter for speculation. To study the recruitment mechanism of MON1-CCZ1 complex to PVCs, we analyzed the interaction of MON1 or CCZ1 with Rab5 in its different nucleotide states via

Y2H. As shown in Figure 5A, MON1 showed interaction with ARA7^{Q69L} and ARA7 but not ARA7^{S24N}. However, CCZ1a and CCZ1b showed little interaction with any form of ARA7. These results demonstrated that MON1 was the direct interacting partner of ARA7 in *Arabidopsis*. Moreover, when YFP-CCZ1a and Myc-MON1 were coexpressed in protoplasts with wild-type, active, or negative ARA7, only the active ARA7 was coimmunoprecipitated with MON1 and CCZ1 to a large degree (Figure 5B),

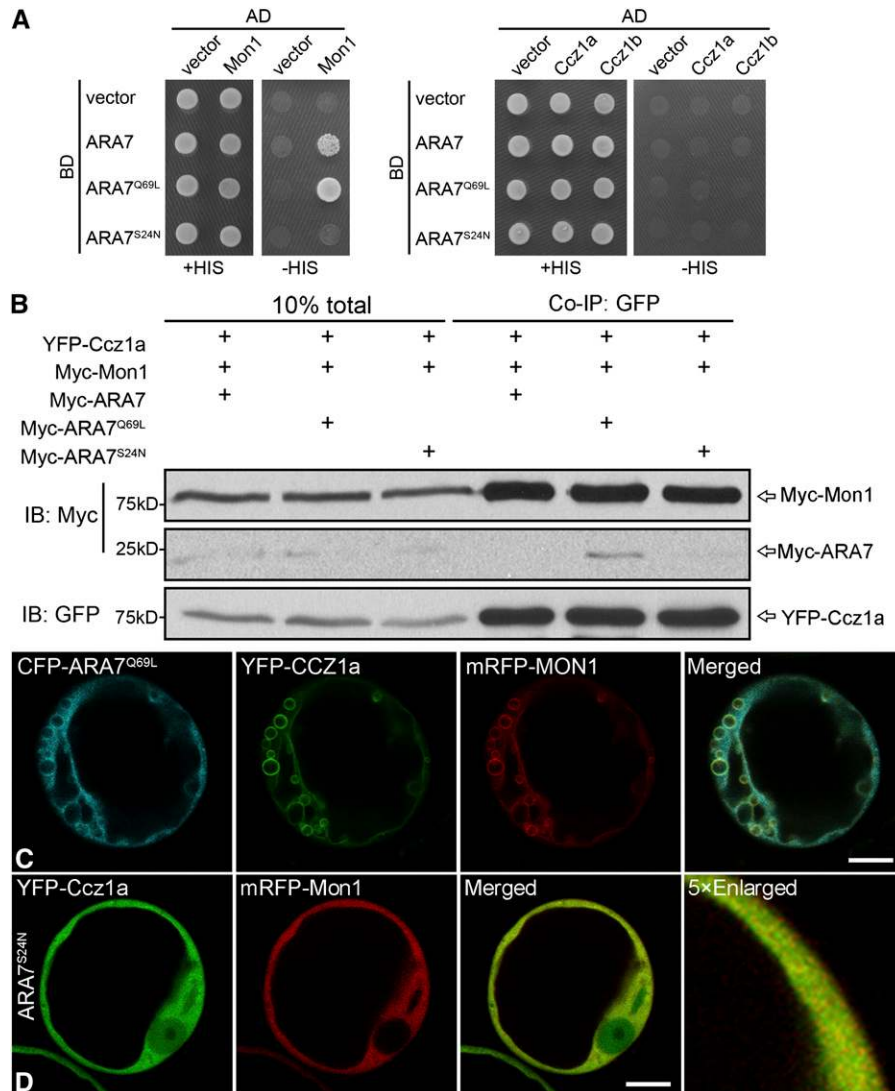


Figure 5. MON1 Directly Interacts with GTP-Bound ARA7, and the MON1-CCZ1 Complex Is Recruited to Enlarged PVCs and the Tonoplast by Active ARA7 in Protoplasts.

(A) Y2H analysis of the interactions among MON1, CCZ1, and different forms of ARA7 (Rab5). MON1, CCZ1a, and CCZ1b were used as prey. Different forms of ARA7 were used as bait. Interactions between two proteins were tested using the HIS3 reporter gene. AD, activation domain; BD, binding domain.

(B) Co-IP assays were performed after transient coexpression of YFP-CCZ1a, Myc-MON1 with wild-type, active, or inactive ARA7 in *Arabidopsis* protoplasts. Total proteins (input) were subjected to immunoprecipitation with GFP-Trap beads followed by immunoblot analysis.

(C) CFP-ARA7^{Q69L} recruited MON1 and CCZ1 complex to the enlarged PVCs and the tonoplast.

(D) The inactive Rab5 (ARA7^{S24N}) did not change the MON1 or CCZ1 pattern. Confocal images were collected from cells at 12 to 14 h after transfection. Bars = 10 μm in **(C)** and **(D)**.

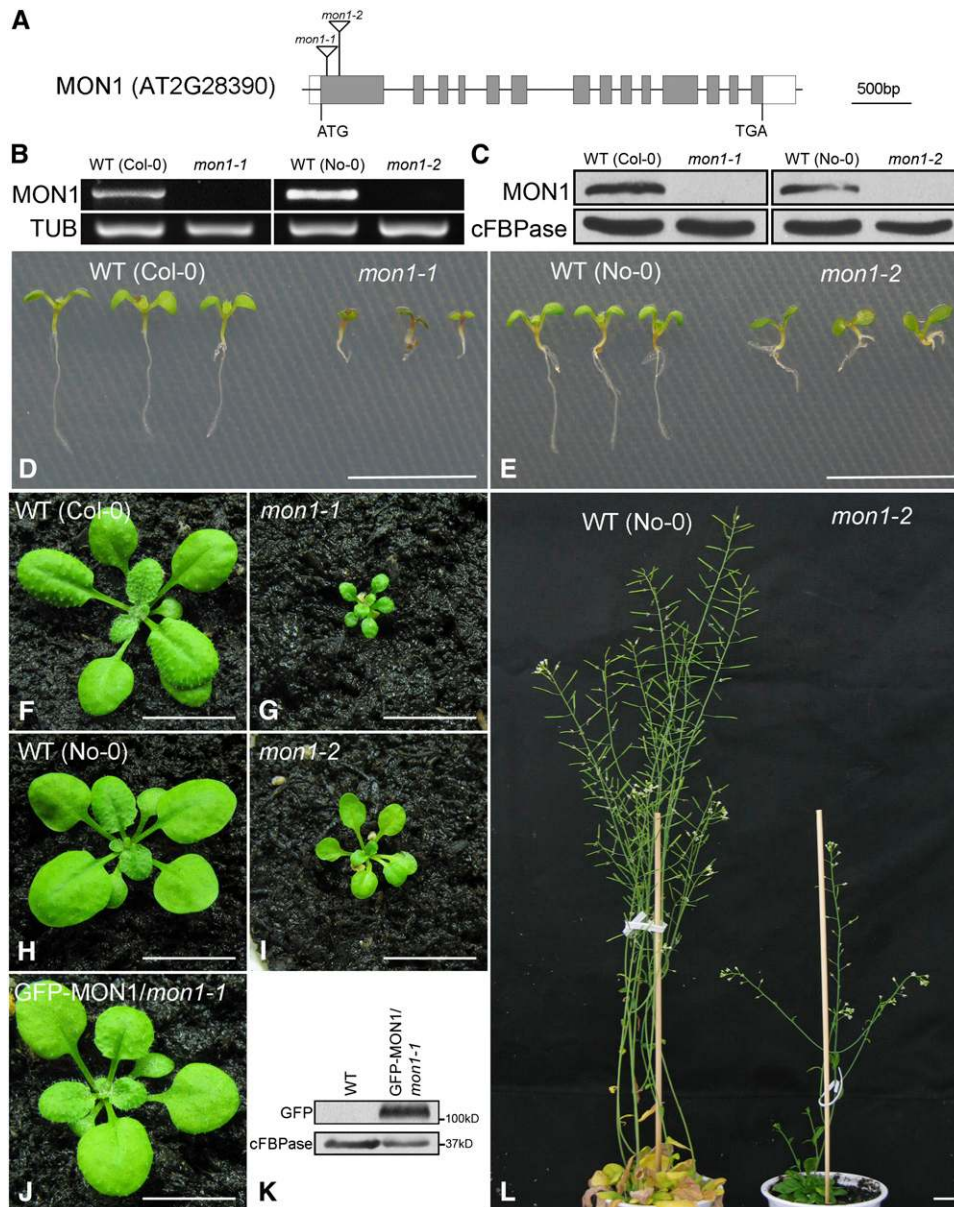


Figure 6. The *mon1* Mutants Show Growth Defects.

(A) Schematic structure of the *MON1* gene and positions of T-DNA insertions.

(B) and **(C)** Mutants were confirmed at the DNA **(B)** and protein **(C)** levels.

(D) and **(E)** The *mon1* mutants showed root growth defects.

(F) to **(I)** The *mon1* mutants showed a growth defect phenotype.

(J) GFP-MON1 recovered the phenotype of *mon1-1*.

(K) Immunoblot showing expression of GFP-MON1 in GFP-MON1/*mon1-1* plants via GFP antibody.

(L) In mature stage, *mon1-2* showed a dwarf phenotype compared with wild-type plants.

Bars = 1 cm in **(D)** to **(J)** and **(L)**.

[See online article for color version of this figure.]

which showed that the MON1-CCZ1 complex preferentially bound to the active ARA7.

We did not detect any wild-type ARA7 in the immunoblot of the Co-IP assay. This might be due to the very transient interaction between wild-type ARA7 and MON1-CCZ1 complex

and relatively low efficiency of the Co-IP detection system. On the other hand, neither MON1 or CCZ1 alone showed interaction with any form of ARA7 (Supplemental Figure 14). Consistent with this, coexpression of the active ARA7 (ARA7^{Q69L}) or CFP-ARA7^{Q69L} with YFP-CCZ1a and mRFP-MON1 showed that

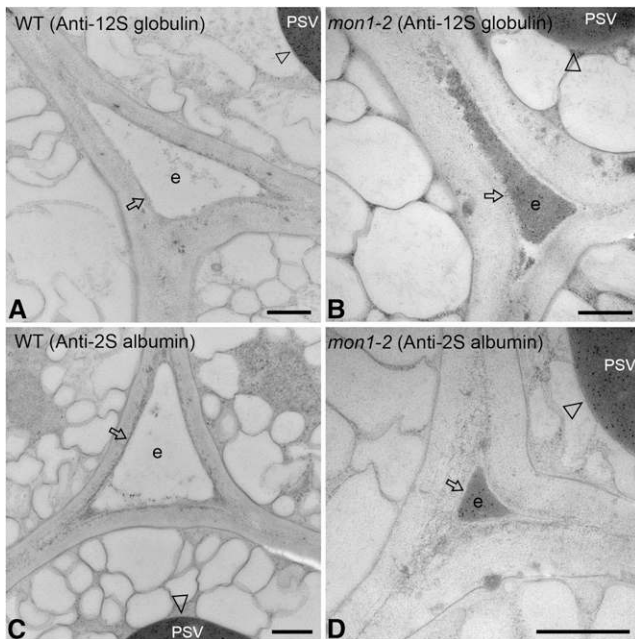


Figure 7. Endogenous Storage Proteins Were Mis-Sorted into the Extracellular Space in *mon1-2* Mutant Seeds.

Immunogold electron microscopy analysis was performed in wild-type (**A**) and **C**) and *mon1-2* mutant (**B**) and **D**) seeds using antibodies against the seed storage proteins 12S globulin (**A**) and **B**) or 2S albumin (**C**) and **D**). Arrowheads indicate PSVs that were positive for both antibodies in wild-type and mutant seeds, while arrows indicate extracellular space positive for labeling only in mutant seeds (arrows in **B**) and **D**). e, extracellular space. Bars = 500 nm.

ARA7^{Q69L} recruited MON1 and CCZ1 complex to the enlarged PVC structures and the tonoplast in protoplasts (Figure 5C; Supplemental Figure 15A).

Overexpression of MON1 and CCZ1a did not cause obvious cytosolic release of YFP-ARA7 (Supplemental Figures 15B and 15C). However, coexpression of the inactive Rab5, ARA7^{S24N}, could not change the cytosolic pattern of MON1 and CCZ1, which excluded the possibility that recruitment of the MON1-CCZ1 complex was induced by the inactive Rab5 (Figure 5D). In addition, expression of MON1 or CCZ1 alone with active Rab5 did not lead to any recruitment of MON1 or CCZ1 to the enlarged PVC structures (Supplemental Figures 15D and 15E). Taken together, we detected a direct interaction between MON1 and active Rab5 and the MON1-CCZ1 complex was recruited to PVCs by active Rab5.

The *mon1* Mutants Showed the Severe Plant Growth Defects

To further study the functional role of the MON1-CCZ1 complex in plant development, two mutant alleles of MON1, *mon1-1* (SALK_075382) and *mon1-2* (54-4894-1), were identified. The *mon1-1* mutant contains a T-DNA insertion in the first exon, while the *mon1-2* harbors a Ds transposon in the first exon (Figure 6A). Both mutants were null mutants, since MON1 was not detected

at either RNA or protein level (Figures 6B and 6C). Similar to the dominant-negative *Rab7* mutant, both *mon1* mutants also showed a short root phenotype (Figures 2A, 2B, 6D, and 6E; Supplemental Figure 16). This indicated that proper Rab7 activation was important for normal root development. Compared with the wild-type plants, both mutants also showed retarded growth (Figures 6F to 6I). The developmental defects of *mon1-1* mutant were complemented by the GFP-MON1 fragment (Figure 6J), and immunoblot using GFP antibody confirmed the successful expression of GFP-MON1 in the *mon1-1* mutant (Figure 6K). At the mature stage, *mon1-2* also showed a dwarf phenotype compared with the wild-type plant (Figure 6L). Thus, MON1 was indispensable for normal plant growth.

Effect of *MON1* Mutation on Vacuolar Transport and Biogenesis

Since previous studies showed that defects in the vacuolar trafficking pathway interfered with proper cargo delivery to the PSVs (Goh et al., 2007; Isono et al., 2010), we next examined vacuolar transport of endogenous storage proteins and PSV marker GFP-CT24 in wild-type and *mon1* mutant seeds. In immunogold transmission electron microscopy studies using antibodies against two storage proteins, both 12S globulin and 2S albumin labels (gold particles) were found exclusively in the PSVs (Figures 7A and 7C, indicated by arrowheads) but missing in the extracellular space (indicated by arrows) in the wild-type seeds. However, in an identical labeling experiment using the *mon1-2* mutant seeds, in addition to PSV labeling by both antibodies (Figures 7B and 7D, indicated by arrowheads), abundant gold particle labeling was found in the electron-dense extracellular space (Figures 7B and 7D, indicated by arrows). These results indicated that mutation of *MON1* caused secretion of storage proteins.

Similarly, as shown in Figures 8A and 8B, GFP-CT24 was found in PSVs in wild-type seeds but was secreted outside of the cells in *mon1-1* mutant seeds, further supporting the conclusion that the *mon1* mutation inhibited vacuolar transport and caused secretion of vacuolar cargoes. GFP-MON1 mainly showed a cytosolic and endosomal pattern in *Arabidopsis* plants (Figure 8C). Upon Wort treatment, GFP-MON1-positive endosomes formed enlarged PVC structures, confirming PVC localization of MON1 (Figure 8D).

To study the possible effects of *MON1* mutation on PVC and vacuole morphology, we introduced PVC and vacuolar markers into the *mon1-1* mutant via genetic crossing. As shown in Figures 8E and 8F, in *mon1-1* mutant roots, YFP-ARA7-labeled PVCs formed enlarged endosomes, a result similar to the effect of RABG3f^{T22N} on PVCs. Fragmented vacuoles were also frequently observed in *mon1-1* mutant roots compared with the wild type (Figures 8G and 8H). Since the MON1-CCZ1 complex served as the Rab5 effector and Rab7 GEF to mediate PVC maturation, we next compared the localizations of Rab5 and Rab7 in the *mon1-1* mutant. Interestingly, the Rab7-positive endosomes were separate from the Rab5 (Ch-RHA1)-labeled enlarged PVCs (Figure 8I). Rab7-positive endosomes were also distinct from the VSR-labeled PVCs in cells coexpressing the *MON1* RNA interference (RNAi) construct (MON1RNAi) with YFP-RABG3f and mRFP-VSR2 (Supplemental Figure 17). Since the *MON1* mutation affected the

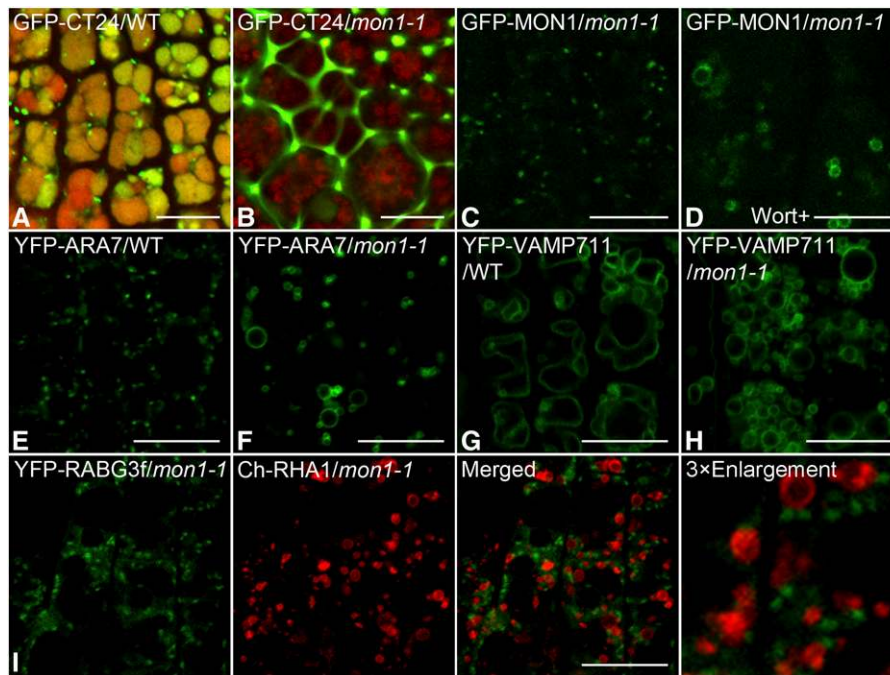


Figure 8. Effects of *MON1* Mutation on Vacuolar Transport and Organelle Markers.

- (A) GFP-CT24 localized to PSV in wild-type seeds.
 (B) GFP-CT24 was secreted in *mon1-1* mutant seeds.
 (C) Localization of GFP-MON1 in *mon1-1* mutant roots.
 (D) GFP-MON1 was sensitive to Wort treatment (33 μ M).
 (E) YFP-ARA7 localized to PVCs in wild-type roots.
 (F) YFP-ARA7 formed enlarged PVCs in *mon1-1* mutant roots.
 (G) YFP-VAMP711 localized to the tonoplast in wild-type roots.
 (H) Localization of YFP-VAMP711 in *mon1-1* mutant roots.
 (I) YFP-RABG3f localized to the endosomes, which were separate from Ch-RHA1-positive enlarged PVCs in *mon1-1* mutant roots.
 Bars = 10 μ m.

proper tonoplast localization of RABG3f and induced ARA7- or VSR-labeled PVCs to form enlarged structures lacking RABG3f, *MON1* may serve as a linker between Rab5 and Rab7 and mediate PVC maturation in *Arabidopsis*.

Identification of PVCs and Vacuoles in Wild-Type, *mon1-2*, and RABG3f^{T22N} Cells

To further identify and confirm the nature of PVCs and vacuoles observed in wild-type, *mon1*, and RABG3f^{T22N} root cells, we next performed immunogold electron microscopy studies with VSR antibodies. Root cells were first subjected to high-pressure freezing/freeze substitution, followed by block preparation and sectioning for immunogold electron microscopy. Different from wild-type cells, fragmented vacuoles and enlarged PVCs were frequently found in cells of *mon1-2* and RABG3f^{T22N} (Figures 9A to 9C). VSR antibodies specifically labeled normal PVCs in wild-type cells and enlarged PVCs in *mon1-2* and RABG3f^{T22N} root cells (Figures 9D to 9F). Statistical analysis showed that the average diameter of PVCs in *mon1-2* and RABG3f^{T22N} was larger than that in wild-type cells (Supplemental Figure 18A). Enlarged PVCs were largely derived from homotypic fusion of PVCs (Supplemental

Figures 18B and 18C), a result similar to ARA7^{Q69L}- and Wort-induced enlarged PVC structures (Wang et al., 2009; Jia et al., 2013). Golgi stacks and the TGN remained normal in both *mon1-2* and RABG3f^{T22N} root cells (Supplemental Figures 18D to 18F). On the other hand, *MON1* antibodies labeled normal PVCs in wild-type cells (Figure 9G). GFP antibodies also labeled normal PVCs in GFP-*MON1/mon1-1*, further confirming PVC localization of *MON1* (Figure 9H). However, due to the dominant-negative mutation of Rab7, *MON1* antibodies strongly labeled the enlarged PVCs in RABG3f^{T22N} root cells (Figure 9I). Taken together, these results demonstrated that (1) *MON1*-mediated Rab7 activation occurred on PVCs and (2) both *mon1* mutations and dominant-negative *rab7* mutations affected proper Rab7 function and caused the formation of enlarged PVCs.

DISCUSSION

Rab7 Activation Is Essential for Vacuolar Trafficking and Biogenesis

In plants, similar to other eukaryotic cells, Rab proteins play vital roles as switches in membrane trafficking system that are essential

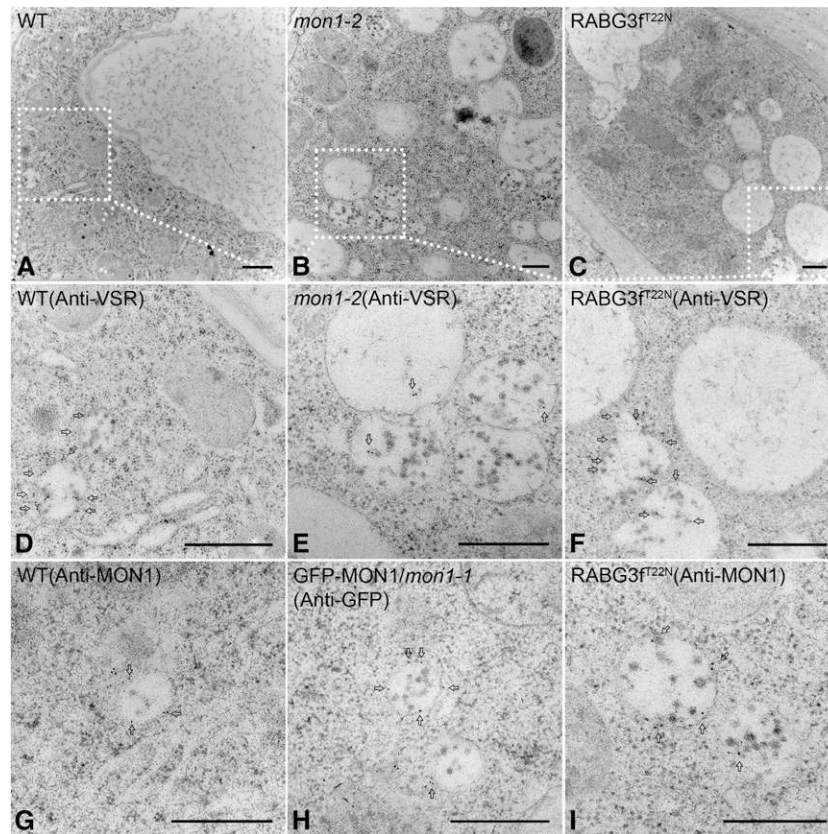


Figure 9. Immunogold Electron Microscopy and Ultrastructural Analysis of PVCs and Vacuoles in Wild-Type, *mon1-2*, and *RABG3f^{T22N}* Root Cells. Immunogold electron microscopy analysis of ultra-thin sections cut from high-pressure frozen/freeze-substituted samples of wild-type, *mon1-2*, and *RABG3f^{T22N}* root cells. (A) to (C) Overview of wild-type, *mon1-2*, and *RABG3f^{T22N}* root cells. (D) to (F) Immunogold electron microscopy analysis with VSR antibodies on normal PVCs in wild-type root cells (D) and enlarged PVCs in *mon1-2* (E) and *RABG3f^{T22N}* (F) root cells. (G) to (I) MON1 antibodies labeled normal PVCs in wild-type root cells (G). GFP antibodies also labeled normal PVCs in GFP-MON1/*mon1-1* root cells (H). MON1 antibodies labeled enlarged PVCs in *RABG3f^{T22N}* root cells (I). Bars = 500 nm in (A) to (I).

for development and growth (Woollard and Moore, 2008; Pfeffer, 2013). Extensive studies of Rab5 in plants demonstrate that Rab5 mainly localizes to PVCs and functions in vacuolar trafficking (Goh et al., 2007; Ebine et al., 2011; Bottanelli et al., 2012; Inoue et al., 2013; Jia et al., 2013). The *Arabidopsis* double mutants of Rab5 (*ara7 rha1*) or mutants lacking functional Rab5 GEF VPS9a are not viable (Goh et al., 2007; Ebine et al., 2011). Rab7 localizes to the tonoplast and may function in the final step of vacuolar trafficking (Vernoud et al., 2003; Mazel et al., 2004). However, little is known about the underlying mechanism of Rab7 activation and its relationship with Rab5 in plants.

Among the eight putative Rab7 homologs in *Arabidopsis*, RABG3f shows prominent expression in different tissues and developmental stages (Vernoud et al., 2003). In this study, RABG3f (Rab7) was localized to PVCs and the tonoplast (Supplemental Figures 2A and 2B), supporting its expected function in the vacuolar pathway. In addition, proper activation of RABG3f is crucial for its correct localization because in contrast with the proper tonoplast

localization of active RABG3f, inactive RABG3f was failed to reach the tonoplast (Figure 1A).

To further illustrate the Rab7 function in vacuolar trafficking, we generated transgenic *Arabidopsis* plants expressing the inactive RABG3f under the control of Dex-inducible promoter. These plants died as seedlings upon Dex induction, demonstrating the indispensable role of Rab7 in plant development (Figure 2A). At the cellular level, enlarged PVCs and fragmented vacuoles were observed, while vacuolar trafficking was also inhibited when inactive Rab7 was expressed (Figures 1C to 1E). Thus, proper activation of Rab7 leads to its function in PVC maturation, vacuole biogenesis, and vacuolar trafficking in plants.

The MON1-CCZ1 Complex Is the Rab7 GEF in Plants

Rab7 activation plays important roles in the membrane trafficking system. However, little is known about the activation mechanism of Rab7 in plants. In yeast, Rab7 is activated by the

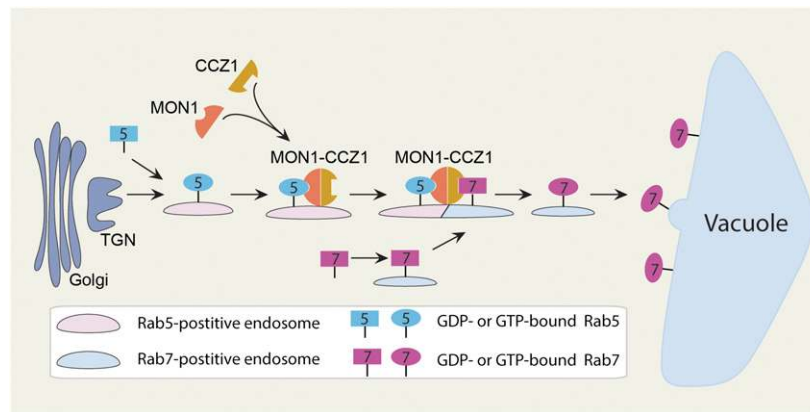


Figure 10. Working Model of the Rab5- and Rab7-Mediated Vacuolar Trafficking Pathway in Plants.

Based on this study, a vacuolar trafficking pathway that involves Rab5 and Rab7 is presented. Rab5 protein is first activated and targeted to PVCs. Then, active Rab5 recruits the MON1-CCZ1 complex. This complex also serves as the Rab7 GEF to mediate Rab5-to-Rab7 conversion on PVCs. Active Rab7 finally mediates the fusion between the PVC and the vacuole.

[See online article for color version of this figure.]

MON1-CCZ1 complex (Nordmann et al., 2010). In this study, we demonstrated that the *Arabidopsis* MON1 and CCZ1 form a dimeric complex and function as the Rab7 GEF. First, we showed that MON1 and CCZ1 interacted with each other to form a complex (Figures 3A and 3B). Then, *in vitro* GEF assays demonstrated the specific GEF activity of MON1-CCZ1 complex toward Rab7 (Figures 3C and 3D). Through Co-IP and localization studies, we also detected preferential binding of MON1-CCZ1 complex to inactive Rab7 on PVCs (Figures 3E, 4B, and 4C). Thus, like in yeast, *Arabidopsis* MON1-CCZ1 complex holds similar GEF function toward Rab7.

The MON1-CCZ1 Complex Mediates Rab5-to-Rab7 Conversion on PVCs in Plants

In plant cells, most vacuolar proteins are sorted at the TGN and transported to the vacuole through PVCs (Lam et al., 2007a). However, the underlying mechanism of PVC-to-vacuole transport is largely unknown in plants. In mammalian cells, it is generally thought that trafficking to the lysosome is accompanied by maturation of endosomal organelles (Rink et al., 2005). Rab5-to-Rab7 conversion triggers maturation of late endosomes from early endosomes, in which the early endosome-localized Rab5 is replaced by MON1-CCZ1 complex, which in turn recruits Rab7, resulting in a Rab7-positive late endosome (Kinchen and Ravichandran, 2010). In plants, Rab5 localizes to PVCs, while Rab7 shows an endosome and tonoplast localization pattern (Geldner et al., 2009).

In this study, we found that the *Arabidopsis* MON1-CCZ1 complex serves as a linker to mediate Rab5-to-Rab7 conversion on PVCs, which is supported by several lines of evidence. (1) The Y2H assay showed direct interaction between MON1 and active Rab5 (Figure 5A), indicating that MON1 was the effector for Rab5. (2) When expressed in protoplasts, MON1-CCZ1 complex was recruited by active Rab5 to PVCs and subsequently recruited the inactive Rab7 (Figures 3E, 4B, 5B, and 5C). (3) In

wild-type cells, Rab5- and Rab7-positive endosomes were partially colocalized (Figure 1B). However, in the *mon1-1* mutant, Rab5-positive endosomes formed enlarged structures that were separate from Rab7-positive endosomes (Figure 8I). (4) Time-lapse imaging further confirmed that Rab7 was recruited to Rab5-positive PVCs for possible Rab conversion events (Supplemental Movie 1 and Supplemental Figure 3). These results indicate that PVC maturation in plants involves a Rab5-to-Rab7 conversion, which is mediated by the MON1-CCZ1 complex (Figure 10).

PVCs Are Maturing Compartments between the TGN to the Vacuole

Recent studies point that PVCs mature from the TGN and ultimately fuse with the vacuole (Scheuring et al., 2011). We agree with this, and in our PVC maturation model, Rab5 mainly induces the homotypic fusion of PVCs (Jia et al., 2013), while Rab7 mediates the fusion between PVCs and vacuoles. The MON1-CCZ1 complex mediates the Rab5-to-Rab7 transition (Figure 10). Expression of RABG3^{T22N} or loss of functional Rab7 GEF inhibits the fusion between PVCs and vacuoles, which results in enlarged PVCs, fragmented vacuoles, and a vacuolar trafficking defect (Figures 1C to 1E, 8A, 8B, and 8E to 8H).

A recent article identified an intermediate compartment situated between PVCs and vacuoles using a recycling-defective VSR in tobacco (*Nicotiana tabacum*) epidermal cells (Foresti et al., 2010). This study is consistent with the concept that PVCs are a series of maturing compartments, but we think that the RHA1-positive late prevacuolar compartments do not represent the final stage of PVC maturation. If RHA1-positive PVCs fuse with vacuoles, we should also detect RHA1 on the tonoplast. However, RHA1 localizes only to PVCs, as also described in other reports (Sohn et al., 2003; Lee et al., 2004; Zelazny et al., 2013). Irrespective of the RHA1 question, PVCs still need to undergo a Rab5-to-Rab7 transition on the PVC membrane before fusing with the vacuole.

Possible Multiple Vacuolar Trafficking Pathways in *Arabidopsis*

Vacuolar trafficking of soluble and membrane cargo requires different classes of small GTPases, including Rab5 and Rab7 families (Bottanelli et al., 2012). In this study, we demonstrated that MON1-CCZ1 mediates the Rab5-to-Rab7 transition, and sequential action of Rab5 and Rab7 regulates PVC maturation in plants (Figure 10). However, combined with previous studies (Bottanelli et al., 2011), the following evidence from this study points to the possible existence of a Rab5-dependent (Rab7-independent) or Rab7-dependent (Rab5-independent) vacuolar pathway in *Arabidopsis*: (1) Expression of Rab7^{T22N} or loss of function of Rab7 GEF protein did not block YFP-VAMP711 from reaching the vacuole (Figures 1D and 8H). (2) YFP-ARA7 reached some small vacuole-like structures besides enlarged PVCs in *mon1* mutant roots (Figure 8F). Thus, multiple vacuolar trafficking pathways may exist in *Arabidopsis*. Another interesting question is the origin of the endosomes containing GDP-bound Rab7. Previous studies suggested that targeting of GDP-bound Rab7 is mediated by the PRA1 family proteins (Rho et al., 2009). The PVC-localized Os-PRA1 was shown to serve as an Os-Rab7 interacting partner and facilitated the delivery of Os-Rab7 to the target membrane (Heo et al., 2010). Since endosome-localized PRA1 family proteins also exist in *Arabidopsis*, GDP-bound Rab7-positive endosomes may be derived from certain portions of PVCs that contain the PRA1 family proteins (Alvim Kamei et al., 2008). Future study of different Rab machineries such as tethering factors and SNAREs will lead to a better understanding of plant vacuolar trafficking pathways.

METHODS

Plasmid Construction

Detailed construct information and primer sequences are listed in Supplemental Tables 1 and 2. For the YFP-RABG3f transgenic plants, the full-length cDNA of *RABG3f* was amplified and cloned into the pBI121 backbone for construction of the YFP fusion (Lam et al., 2007b). For the RABG3f and RABG3f^{T22N} transgenic plants, *RABG3f* and *RABG3f*^{T22N} were amplified and cloned into the pTA7002 backbone for construction of the Myc fusion. For the GFP-RABG3f, GFP-RABG3f^{Q67L}, and GFP-RABG3f^{T22N} transgenic plants, GFP fusions of Rab7 mutants were cloned into the pTA7002 backbone for construction and generation of transgenic plants (Aoyama and Chua, 1997). For the GFP-MON1/*mon1-1* transgenic plant, *MON1* was cloned into the pUBN-GFP-DEST vector for transformation (Grefen et al., 2010). For the *MON1* RNAi construct, a 600-bp sequence of *MON1* predicted using MatchPoint (<http://plantindustry.csiro.au/RNAi/software.htm>) was cloned into the pHANNIBAL vector. All constructs were confirmed by restriction mapping and DNA sequencing.

Plant Materials and Growth Conditions

To generate the transgenic plants, all constructs were introduced into *Agrobacterium tumefaciens* and transformed into wild-type *Arabidopsis thaliana* plants by the floral dip method (Clough and Bent, 1998).

The T-DNA insertion lines SALK_075382 (*mon1-1*) was obtained from the ABRC (Alonso et al., 2003). The *Arabidopsis* Ds transposon *mon1-2* (54-4894-1) mutant line was obtained from RIKEN (Sakurai et al., 2005).

The *Arabidopsis* WAVE lines expressing XFP fusions for the Golgi (WAVE22), PVC (WAVE2 and WAVE7), recycling endosome (WAVE34), and the tonoplast (WAVE9) were obtained from the European Arabidopsis

Stock Center (Geldner et al., 2009). The following previously published marker lines were crossed into the dominant-negative *rab7* mutant: the TGN marker line (VHA1-GFP), the PVC marker line (GFP-VSR1), the PM marker line (GFP-LTi6a), the PSV marker line (GFP-CT24), the lytic vacuole marker line (spL-RFP) (Dettmer et al., 2006; Miao et al., 2006; Hunter et al., 2007; Zhang et al., 2011).

Seedlings were grown under continuous light on standard Murashige and Skoog growth medium supplemented with 1% sucrose; adult plants were grown on soil. When indicated, 10 μ M Dex (Sigma-Aldrich) was added to the medium. For nitrogen supplementation experiments, seeds were germinated on medium containing 60 mM nitrogen as previously described (Martin et al., 2002). The molar ratio of KNO₃ to NH₄NO₃ was maintained in each medium as it was in Murashige and Skoog medium (Murashige and Skoog, 1962).

Transient Expression and Confocal Microscopy Images

Maintenance of *Arabidopsis* suspension-cultured cells and transient expression methods were described previously (Tse et al., 2004; Miao and Jiang, 2007; Gao et al., 2012; Zhuang et al., 2013). Confocal images were collected at 12 to 14 h or 36 to 48 h after transformation as indicated using an Olympus FV1000 system. Images were processed using Adobe Photoshop as described previously (Jiang and Rogers, 1998; Shen et al., 2013a). Time-lapse movie and images were obtained by spinning disc confocal microscopy (Andor) and analyzed by Imaris software (Bitplane) as described previously (Wang et al., 2010; Ding et al., 2014).

Drug Treatments

For drug treatment experiment, aliquots of Wort solution (Sigma-Aldrich; stock at 1.65 mM in dimethyl sulphoxide) were added to the medium to a final concentration of 33 μ M.

Yeast Two-Hybrid Assay

The cDNAs for *MON1*, *CCZ1a*, and *CCZ1b* were cloned into the pGADT7 AD vector or pGBKT7 DNA-BD vector, and the different forms of Rab5 (*ARA7*) were cloned into the pGBKT7 DNA-BD vector. Plasmids were transformed into the yeast strain AH109. Empty vectors were used for negative controls. At least three colonies were checked for interaction for each transformation.

Immunoprecipitation of GFP-Tagged or Myc-Tagged Proteins

Co-IP methods using GFP-TRAP agarose beads (ChromoTek) or sc-40 AC agarose beads (Santa Cruz Biotechnology) were described previously (Cai et al., 2012).

Expression and Purification of Recombinant Proteins

Plasmids pGEX-GST-CCZ1a-12 \times His-MON1 for coexpression of MON1 and CCZ1a, pGEX-GST-RABG3f, and pGEX-GST-RHA1 were transformed in BL21 Rosetta for expression. The expression of the fusion proteins was induced by the addition of 0.8 mM isopropyl-D-thiogalactoside overnight at 28°C. GST-tagged RABG3f and RHA1 were purified on a 5-mL GST Trap HP column using an ÄKTA TM purifier (Amersham Biosciences). GST-tagged CCZ1a-12 \times His-MON1 protein was purified on a 5-mL GST Trap HP column, followed by an additional purification on a 5-mL HisTrap HP column. Buffer exchange and protein concentration were performed with an Amicon Ultra-4 centrifugal filter (Millipore).

Nucleotide-Exchange Assay

Intrinsic tryptophan fluorescence measurements were performed as described previously (Pan et al., 1995; Antony et al., 2001; Goh et al., 2007).

Briefly, tryptophan fluorescence was recorded at 340 nm upon excitation at 298 nm by a fluorescence spectrophotometer (model F-7000; Hitachi High Technologies). All experiments were performed at 25°C in reaction buffer (20 mM Tris-HCl, pH 8.0, 150 mM NaCl, and 0.5 mM MgCl₂). Each purified Rab protein was preloaded with GDP and incubated with or without GST-CCZ1a-12×His-MON1. Then, GMP-PNP was added to 0.1 mM at time 0 and mixed for 10 s before fluorescence records. Tryptophan fluorescence at time 0 was set at 1. On the figures, y axes show arbitrary units representing relative fluorescence levels. The trend lines were created using OriginPro 8.0 (OriginLab). The assay was repeated at least three times for each Rab GTPase.

Antibodies

A synthetic peptide (SRSSPSSDTEFADPNPSSDPETNSERVQSQLEC) within the N terminus of *Arabidopsis* MON1 was synthesized (GenScript) and used as antigen to raise antibodies as described previously (Lam et al., 2007c). Myc antibodies were purchased from Santa Cruz Biotechnology (catalog No. sc-789) and used at 0.2 μg/mL for immunoblot analysis. GFP, 12S, 2S, and Aleurain antibodies were described previously (Shimada et al., 2003; Tse et al., 2006).

Transmission Electron Microscopy Study

The general procedures for transmission electron microscopy sample preparation, thin sectioning, and immunogold labeling were performed essentially as described previously (Tse et al., 2004; Lam et al., 2007c; Wang et al., 2010). Immunogold labeling was performed with antibodies against VSR (40 mg/mL) (Tse et al., 2004), MON1 (40 mg/mL), 12S globulin (dilution 1:2000), 2S albumin (dilution 1:2000) (Shimada et al., 2003), and gold-coupled secondary antibody at a 1:50 dilution.

Accession Numbers

The *Arabidopsis* Genome Initiative locus identifiers for the genes mentioned in this article are *RABG3f* (At3g18820), *MON1* (At2g28390), *CCZ1a* (At1g16020), *CCZ1b* (At1g80910), *ARA7* (AT4G19640), and *RHA1* (AT5G45130). Sequence data from the alignment of MON1 and CCZ1 can be found in the GenBank data library under accession numbers *Mon1p* (*Saccharomyces cerevisiae*) (NP_011391.2), *SAND-1* (*Caenorhabditis elegans*) (NP_500791.2), *O1g0976000* (*Oryza sativa*) (NP_001045563.2), *Ccz1p* (*S. cerevisiae*) (NP_009689.3), *CCZ-1* (*C. elegans*) (NP_506387.1), and *08g0427300* (*O. sativa*) (NP_001061842.1).

Supplemental Data

The following materials are available in the online version of this article.

Supplemental Figure 1. Transgenic Plants Used in This Study.

Supplemental Figure 2. RABG3f, an *Arabidopsis* Rab7 Homolog, Localizes to PVCs and the Tonoplast in *Arabidopsis* Cells.

Supplemental Figure 3. Examples of 4D (3D Image Plus Time) Imaging of Likely RABG3f Recruitment to RHA1-Positive PVCs.

Supplemental Figure 4. Dominant-Negative RABG3f Induces PVCs to Form Enlarged Structures and Has No Effect on Other Organelle Markers.

Supplemental Figure 5. Identification of RABG3f^{T22N} Induced Enlarged Endosomes in Transient Expression System.

Supplemental Figure 6. Different Lines of Dominant-Negative RABG3f Mutants and Dex Dosage-Dependent Phenotypes of RABG3f^{T22N}.

Supplemental Figure 7. Dominant-Negative RABG3f Mutant Protein Affects Degradation of Storage Proteins in PSV and the Effect of Nitrogen Treatment.

Supplemental Figure 8. The *Arabidopsis* MON1 and CCZ1 Proteins and Their Homologs.

Supplemental Figure 9. Characterization of MON1 Antibodies and Interaction between Inactive RABG3f and MON1 in Transgenic Plants.

Supplemental Figure 10. Purified MON1-CCZ1, RABG3f, and RHA1 Proteins for in Vitro GEF Assays Were Subjected to SDS-PAGE Followed by Coomassie Blue Staining.

Supplemental Figure 11. Neither MON1 nor CCZ1a Binds to Any Form of RABG3f in Protoplasts.

Supplemental Figure 12. Time-Course Analysis of MON1 and CCZ1 Recruitment in Protoplasts.

Supplemental Figure 13. Identification of RABG3f^{T22N}-Induced, MON1-CCZ1-Localized Enlarged PVCs in Transient Expression System.

Supplemental Figure 14. Neither MON1 nor CCZ1a Bind to Any Form of ARA7 in Protoplasts.

Supplemental Figure 15. Subcellular Localization Study of MON1, CCZ1, ARA7, and ARA7^{Q69L} in Protoplasts.

Supplemental Figure 16. Root Length of 6-d-old Wild-Type, *mon1-1*, and *mon1-2* Mutant Plants.

Supplemental Figure 17. Effect of Knockdown of *MON1* on Organelle Markers in Transient Expression System.

Supplemental Figure 18. Ultrastructural Analysis of PVC, Golgi, and TGN in Wild-Type, *mon1-2*, and RABG3f^{T22N} Root Cells.

Supplemental Table 1. Constructs Used in This Study.

Supplemental Table 2. Primers Used in This Study.

Supplemental Movie 1. Examples of Time-Lapse Imaging of Root Cells Expressing YFP-RABG3f and Ch-RHA1.

ACKNOWLEDGMENTS

This work was supported by grants from the Research Grants Council of Hong Kong (CUHK466610, 466011, 465112, 466613, CUHK2/CRF/11G, HKUST10/CRF/12R, and AoE/M-05/12), by the NSFC/RGC (N_CUHK406/12), by the NSFC (31270226), and by the Shenzhen Peacock Project (KQTD201101) to L.J.

AUTHOR CONTRIBUTIONS

Y.C. and L.J. conceived and designed the experiments. Y.C. and Q.Z. performed the experiments. Y.C., Q.Z., C.G., Y.D., and Y.Z. analyzed the data. Y.C., Q.Z., T.U., A.N., and L.J. discussed and commented on the content of the article. Y.C., Q.Z., and L.J. wrote the article.

Received January 16, 2014; revised April 12, 2014; accepted April 22, 2014; published May 13, 2014.

REFERENCES

- Alonso, J.M., et al. (2003). Genome-wide insertional mutagenesis of *Arabidopsis thaliana*. *Science* **301**: 653–657.
- Alvim Kamei, C.L., Boruc, J., Vandepoele, K., Van den Daele, H., Maes, S., Russinova, E., Inzé, D., and De Veylder, L. (2008). The PRA1 gene family in *Arabidopsis*. *Plant Physiol.* **147**: 1735–1749.

- Antonny, B., Madden, D., Hamamoto, S., Orci, L., and Schekman, R.** (2001). Dynamics of the COPII coat with GTP and stable analogues. *Nat. Cell Biol.* **3**: 531–537.
- Aoyama, T., and Chua, N.H.** (1997). A glucocorticoid-mediated transcriptional induction system in transgenic plants. *Plant J.* **11**: 605–612.
- Belenkaya, T.Y., Wu, Y., Tang, X., Zhou, B., Cheng, L., Sharma, Y.V., Yan, D., Selva, E.M., and Lin, X.** (2008). The retromer complex influences Wnt secretion by recycling wntless from endosomes to the trans-Golgi network. *Dev. Cell* **14**: 120–131.
- Bottanelli, F., Foresti, O., Hanton, S., and Denecke, J.** (2011). Vacuolar transport in tobacco leaf epidermis cells involves a single route for soluble cargo and multiple routes for membrane cargo. *Plant Cell* **23**: 3007–3025.
- Bottanelli, F., Gershlick, D.C., and Denecke, J.** (2012). Evidence for sequential action of Rab5 and Rab7 GTPases in prevacuolar organelle partitioning. *Traffic* **13**: 338–354.
- Cai, H., Reinisch, K., and Ferro-Novick, S.** (2007). Coats, tethers, Rabs, and SNAREs work together to mediate the intracellular destination of a transport vesicle. *Dev. Cell* **12**: 671–682.
- Cai, Y., Zhuang, X., Wang, J., Wang, H., Lam, S.K., Gao, C., Wang, X., and Jiang, L.** (2012). Vacuolar degradation of two integral plasma membrane proteins, AtLRR84A and OsSCAMP1, is cargo ubiquitination-independent and prevacuolar compartment-mediated in plant cells. *Traffic* **13**: 1023–1040.
- Chow, C.M., Neto, H., Foucart, C., and Moore, I.** (2008). Rab-A2 and Rab-A3 GTPases define a trans-Golgi endosomal membrane domain in *Arabidopsis* that contributes substantially to the cell plate. *Plant Cell* **20**: 101–123.
- Clough, S.J., and Bent, A.F.** (1998). Floral dip: a simplified method for *Agrobacterium*-mediated transformation of *Arabidopsis thaliana*. *Plant J.* **16**: 735–743.
- Collette, J.R., Chi, R.J., Boettner, D.R., Fernandez-Golbano, I.M., Plemel, R., Merz, A.J., Geli, M.I., Traub, L.M., and Lemmon, S.K.** (2009). Clathrin functions in the absence of the terminal domain binding site for adaptor-associated clathrin-box motifs. *Mol. Biol. Cell* **20**: 3401–3413.
- daSilva, L.L., Foresti, O., and Denecke, J.** (2006). Targeting of the plant vacuolar sorting receptor BP80 is dependent on multiple sorting signals in the cytosolic tail. *Plant Cell* **18**: 1477–1497.
- Dettmer, J., Hong-Hermesdorf, A., Stierhof, Y.D., and Schumacher, K.** (2006). Vacuolar H⁺-ATPase activity is required for endocytic and secretory trafficking in *Arabidopsis*. *Plant Cell* **18**: 715–730.
- Ding, Y., Wang, J., Chun Lai, J.H., Ling Chan, V.H., Wang, X., Cai, Y., Tan, X., Bao, Y., Xia, J., Robinson, D.G., and Jiang, L.** (2014). Exo70E2 is essential for exocyst subunit recruitment and EXPO formation in both plants and animals. *Mol. Biol. Cell* **25**: 412–426.
- Ebine, K., Okatani, Y., Uemura, T., Goh, T., Shoda, K., Niihama, M., Morita, M.T., Spitzer, C., Otegui, M.S., Nakano, A., and Ueda, T.** (2008). A SNARE complex unique to seed plants is required for protein storage vacuole biogenesis and seed development of *Arabidopsis thaliana*. *Plant Cell* **20**: 3006–3021.
- Ebine, K., et al.** (2011). A membrane trafficking pathway regulated by the plant-specific RAB GTPase ARA6. *Nat. Cell Biol.* **13**: 853–859.
- Foresti, O., Gershlick, D.C., Bottanelli, F., Hummel, E., Hawes, C., and Denecke, J.** (2010). A recycling-defective vacuolar sorting receptor reveals an intermediate compartment situated between prevacuoles and vacuoles in tobacco. *Plant Cell* **22**: 3992–4008.
- Geldner, N., Dénervaud-Tendon, V., Hyman, D.L., Mayer, U., Stierhof, Y.D., and Chory, J.** (2009). Rapid, combinatorial analysis of membrane compartments in intact plants with a multicolor marker set. *Plant J.* **59**: 169–178.
- Gao, C., Yu, C.K., Qu, S., San, M.W., Li, K.Y., Lo, S.W., and Jiang, L.** (2012). The Golgi-localized *Arabidopsis* endomembrane protein12 contains both endoplasmic reticulum export and Golgi retention signals at its C terminus. *Plant Cell* **24**: 2086–2104.
- Goh, T., Uchida, W., Arakawa, S., Ito, E., Dainobu, T., Ebine, K., Takeuchi, M., Sato, K., Ueda, T., and Nakano, A.** (2007). VPS9a, the common activator for two distinct types of Rab5 GTPases, is essential for the development of *Arabidopsis thaliana*. *Plant Cell* **19**: 3504–3515.
- Grefen, C., Donald, N., Hashimoto, K., Kudla, J., Schumacher, K., and Blatt, M.R.** (2010). A ubiquitin-10 promoter-based vector set for fluorescent protein tagging facilitates temporal stability and native protein distribution in transient and stable expression studies. *Plant J.* **64**: 355–365.
- Heo, J.B., Bang, W.Y., Kim, S.W., Hwang, S.M., Son, Y.S., Im, C.H., Acharya, B.R., Kim, C.W., Kim, S.W., Lee, B.H., and Bahk, J.D.** (2010). OsPRA1 plays a significant role in targeting of OsRab7 into the tonoplast via the prevacuolar compartment during vacuolar trafficking in plant cells. *Planta* **232**: 861–871.
- Holwerda, B.C., Padgett, H.S., and Rogers, J.C.** (1992). Proaleurain vacuolar targeting is mediated by short contiguous peptide interactions. *Plant Cell* **4**: 307–318.
- Hunter, P.R., Craddock, C.P., Di Benedetto, S., Roberts, L.M., and Frigerio, L.** (2007). Fluorescent reporter proteins for the tonoplast and the vacuolar lumen identify a single vacuolar compartment in *Arabidopsis* cells. *Plant Physiol.* **145**: 1371–1382.
- Hwang, I., and Robinson, D.G.** (2009). Transport vesicle formation in plant cells. *Curr. Opin. Plant Biol.* **12**: 660–669.
- Inoue, T., Kondo, Y., Naramoto, S., Nakano, A., and Ueda, T.** (2013). RAB5 activation is required for multiple steps in *Arabidopsis thaliana* root development. *Plant Cell Physiol.* **54**: 1648–1659.
- Isono, E., Katsiarimpa, A., Müller, I.K., Anzenberger, F., Stierhof, Y.D., Geldner, N., Chory, J., and Schwechheimer, C.** (2010). The deubiquitinating enzyme AMSH3 is required for intracellular trafficking and vacuole biogenesis in *Arabidopsis thaliana*. *Plant Cell* **22**: 1826–1837.
- Jia, T., Gao, C., Cui, Y., Wang, J., Ding, Y., Cai, Y., Ueda, T., Nakano, A., and Jiang, L.** (2013). ARA7(Q69L) expression in transgenic *Arabidopsis* cells induces the formation of enlarged multivesicular bodies. *J. Exp. Bot.* **64**: 2817–2829.
- Jiang, L., and Rogers, J.C.** (1998). Integral membrane protein sorting to vacuoles in plant cells: evidence for two pathways. *J. Cell Biol.* **143**: 1183–1199.
- Jiang, L., and Rogers, J.C.** (1999). Sorting of membrane proteins to vacuoles in plant cells. *Plant Sci.* **146**: 55–67.
- Jiang, L., and Sun, S.S.M.** (2002). Membrane anchors for vacuolar targeting: application in plant bioreactors. *Trends Biotechnol.* **20**: 99–102.
- Kincaid, M.M., and Cooper, A.A.** (2007). Misfolded proteins traffic from the endoplasmic reticulum (ER) due to ER export signals. *Mol. Biol. Cell* **18**: 455–463.
- Kinchen, J.M., and Ravichandran, K.S.** (2010). Identification of two evolutionarily conserved genes regulating processing of engulfed apoptotic cells. *Nature* **464**: 778–782.
- Kirsch, T., Paris, N., Butler, J.M., Beevers, L., and Rogers, J.C.** (1994). Purification and initial characterization of a potential plant vacuolar targeting receptor. *Proc. Natl. Acad. Sci. USA* **91**: 3403–3407.
- Kwon, S.I., Cho, H.J., Jung, J.H., Yoshimoto, K., Shirasu, K., and Park, O.K.** (2010). The Rab GTPase RabG3b functions in autophagy and contributes to tracheary element differentiation in *Arabidopsis*. *Plant J.* **64**: 151–164.
- Lam, S.K., Siu, C.L., Hillmer, S., Jang, S., An, G.H., Robinson, D.G., and Jiang, L.** (2007b). Rice SCAMP1 defines clathrin-coated, trans-golgi-located tubular-vesicular structures as an early endosome in tobacco BY-2 cells. *Plant Cell* **19**: 296–319.

- Lam, S.K., Tse, Y.C., Miao, Y., Li, H.Y., Wang, J., Lo, S.W., and Jiang, L. (2007c). Molecular characterization of plant prevacuolar and endosomal compartments. *J. Integr. Plant Biol.* **49**: 1119–1128.
- Lam, S.K., Tse, Y.C., Robinson, D.G., and Jiang, L. (2007a). Tracking down the elusive early endosome. *Trends Plant Sci.* **12**: 497–505.
- Lee, G.J., Sohn, E.J., Lee, M.H., and Hwang, I. (2004). The *Arabidopsis* rab5 homologs rha1 and ara7 localize to the prevacuolar compartment. *Plant Cell Physiol.* **45**: 1211–1220.
- Limpens, E., Ivanov, S., van Esse, W., Voets, G., Fedorova, E., and Bisseling, T. (2009). Medicago N₂-fixing symbiosomes acquire the endocytic identity marker Rab7 but delay the acquisition of vacuolar identity. *Plant Cell* **21**: 2811–2828.
- Markgraf, D.F., Peplowska, K., and Ungermann, C. (2007). Rab cascades and tethering factors in the endomembrane system. *FEBS Lett.* **581**: 2125–2130.
- Martin, T., Oswald, O., and Graham, I.A. (2002). *Arabidopsis* seedling growth, storage lipid mobilization, and photosynthetic gene expression are regulated by carbon:nitrogen availability. *Plant Physiol.* **128**: 472–481.
- Mazel, A., Leshem, Y., Tiwari, B.S., and Levine, A. (2004). Induction of salt and osmotic stress tolerance by overexpression of an intracellular vesicle trafficking protein AtRab7 (AtRabG3e). *Plant Physiol.* **134**: 118–128.
- Miao, Y., and Jiang, L. (2007). Transient expression of fluorescent fusion proteins in protoplasts of suspension cultured cells. *Nat. Protoc.* **2**: 2348–2353.
- Miao, Y., Yan, P.K., Kim, H., Hwang, I., and Jiang, L. (2006). Localization of green fluorescent protein fusions with the seven *Arabidopsis* vacuolar sorting receptors to prevacuolar compartments in tobacco BY-2 cells. *Plant Physiol.* **142**: 945–962.
- Mo, B., Tse, Y.C., and Jiang, L. (2006). Plant prevacuolar/endosomal compartments. *Int. Rev. Cytol.* **253**: 95–129.
- Murashige, T., and Skoog, F. (1962). A revised medium for rapid growth and bio assays with tobacco tissue cultures. *Physiol. Plant.* **15**: 473–497.
- Nahm, M.Y., Kim, S.W., Yun, D., Lee, S.Y., Cho, M.J., and Bahk, J.D. (2003). Molecular and biochemical analyses of OsRab7, a rice Rab7 homolog. *Plant Cell Physiol.* **44**: 1341–1349.
- Nielsen, E., Cheung, A.Y., and Ueda, T. (2008). The regulatory RAB and ARF GTPases for vesicular trafficking. *Plant Physiol.* **147**: 1516–1526.
- Niemes, S., Langhans, M., Viotti, C., Scheuring, D., San Wan Yan, M., Jiang, L., Hillmer, S., Robinson, D.G., and Pimpl, P. (2010). Retromer recycles vacuolar sorting receptors from the trans-Golgi network. *Plant J.* **61**: 107–121.
- Nordmann, M., Cabrera, M., Perz, A., Bröcker, C., Ostrowicz, C., Engelbrecht-Vandré, S., and Ungermann, C. (2010). The Mon1-Ccz1 complex is the GEF of the late endosomal Rab7 homolog Ypt7. *Curr. Biol.* **20**: 1654–1659.
- Novick, P., Medkova, M., Dong, G., Hutagalung, A., Reinisch, K., and Grosshans, B. (2006). Interactions between Rabs, tethers, SNAREs and their regulators in exocytosis. *Biochem. Soc. Trans.* **34**: 683–686.
- Pan, J.Y., Sanford, J.C., and Wessling-Resnick, M. (1995). Effect of guanine nucleotide binding on the intrinsic tryptophan fluorescence properties of Rab5. *J. Biol. Chem.* **270**: 24204–24208.
- Pfeffer, S.R. (2013). Rab GTPase regulation of membrane identity. *Curr. Opin. Cell Biol.* **25**: 414–419.
- Poteryaev, D., Datta, S., Ackema, K., Zerial, M., and Spang, A. (2010). Identification of the switch in early-to-late endosome transition. *Cell* **141**: 497–508.
- Poteryaev, D., Fares, H., Bowerman, B., and Spang, A. (2007). *Caenorhabditis elegans* SAND-1 is essential for RAB-7 function in endosomal traffic. *EMBO J.* **26**: 301–312.
- Qiu, Q.S. (2012). V-ATPase, ScNhx1p and yeast vacuole fusion. *J. Genet. Genomics* **39**: 167–171.
- Rho, H.S., Heo, J.B., Bang, W.Y., Hwang, S.M., Nahm, M.Y., Kwon, H.J., Kim, S.W., Lee, B.H., and Bahk, J.D. (2009). The role of OsPRA1 in vacuolar trafficking by OsRab GTPases in plant system. *Plant Sci.* **177**: 411–417.
- Rink, J., Ghigo, E., Kalaidzidis, Y., and Zerial, M. (2005). Rab conversion as a mechanism of progression from early to late endosomes. *Cell* **122**: 735–749.
- Robinson, D.G., and Pimpl, P. (2014). Receptor-mediated transport of vacuolar proteins: a critical analysis and a new model. *Protoplasma* **251**: 247–264.
- Robinson, D.G., Pimpl, P., Scheuring, D., Stierhof, Y.D., Sturm, S., and Viotti, C. (2012). Trying to make sense of retromer. *Trends Plant Sci.* **17**: 431–439.
- Rogers, S.W., Burks, M., and Rogers, J.C. (1997). Monoclonal antibodies to barley aleurain and homologs from other plants. *Plant J.* **11**: 1359–1368.
- Sakurai, T., Satou, M., Akiyama, K., Iida, K., Seki, M., Kuromori, T., Ito, T., Konagaya, A., Toyoda, T., and Shinozaki, K. (2005). RARGE: a large-scale database of RIKEN *Arabidopsis* resources ranging from transcriptome to phenome. *Nucleic Acids Res.* **33**: D647–D650.
- Scheuring, D., Viotti, C., Krüger, F., Künzl, F., Sturm, S., Bubeck, J., Hillmer, S., Frigerio, L., Robinson, D.G., Pimpl, P., and Schumacher, K. (2011). Multivesicular bodies mature from the trans-Golgi network/early endosome in *Arabidopsis*. *Plant Cell* **23**: 3463–3481.
- Shen, J., Suen, P.K., Wang, X., Lin, Y., Lo, S.W., Rojo, E., and Jiang, L. (2013a). An in vivo expression system for the identification of cargo proteins of vacuolar sorting receptors in *Arabidopsis* culture cells. *Plant J.* **75**: 1003–1017.
- Shen, J., Zeng, Y., Zhuang, X., Sun, L., Yao, X., Pimpl, P., and Jiang, L. (2013b). Organelle pH in the *Arabidopsis* endomembrane system. *Mol. Plant* **6**: 1419–1437.
- Shimada, T., Fuji, K., Tamura, K., Kondo, M., Nishimura, M., and Hara-Nishimura, I. (2003). Vacuolar sorting receptor for seed storage proteins in *Arabidopsis thaliana*. *Proc. Natl. Acad. Sci. USA* **100**: 16095–16100.
- Sohn, E.J., Kim, E.S., Zhao, M., Kim, S.J., Kim, H., Kim, Y.W., Lee, Y.J., Hillmer, S., Sohn, U., Jiang, L., and Hwang, I. (2003). Rha1, an *Arabidopsis* Rab5 homolog, plays a critical role in the vacuolar trafficking of soluble cargo proteins. *Plant Cell* **15**: 1057–1070.
- Stenmark, H. (2009). Rab GTPases as coordinators of vesicle traffic. *Nat. Rev. Mol. Cell Biol.* **10**: 513–525.
- Toyooka, K., Goto, Y., Asatsuma, S., Koizumi, M., Mitsui, T., and Matsuoka, K. (2009). A mobile secretory vesicle cluster involved in mass transport from the Golgi to the plant cell exterior. *Plant Cell* **21**: 1212–1229.
- Tse, Y.C., Lo, S.W., Hillmer, S., Dupree, P., and Jiang, L. (2006). Dynamic response of prevacuolar compartments to brefeldin A in plant cells. *Plant Physiol.* **142**: 1442–1459.
- Tse, Y.C., Mo, B., Hillmer, S., Zhao, M., Lo, S.W., Robinson, D.G., and Jiang, L. (2004). Identification of multivesicular bodies as prevacuolar compartments in *Nicotiana tabacum* BY-2 cells. *Plant Cell* **16**: 672–693.
- Vernoud, V., Horton, A.C., Yang, Z., and Nielsen, E. (2003). Analysis of the small GTPase gene superfamily of *Arabidopsis*. *Plant Physiol.* **131**: 1191–1208.
- Viotti, C., et al. (2010). Endocytic and secretory traffic in *Arabidopsis* merge in the trans-Golgi network/early endosome, an independent and highly dynamic organelle. *Plant Cell* **22**: 1344–1357.
- Vitale, A., and Raikhel, N.V. (1999). What do proteins need to reach different vacuoles? *Trends Plant Sci.* **4**: 149–155.

- Wang, J., Cai, Y., Miao, Y., Lam, S.K., and Jiang, L.** (2009). Wortmannin induces homotypic fusion of plant prevacuolar compartments. *J. Exp. Bot.* **60**: 3075–3083.
- Wang, J., Ding, Y., Wang, J., Hillmer, S., Miao, Y., Lo, S.W., Wang, X., Robinson, D.G., and Jiang, L.** (2010). EXPO, an exocyst-positive organelle distinct from multivesicular endosomes and autophagosomes, mediates cytosol to cell wall exocytosis in *Arabidopsis* and tobacco cells. *Plant Cell* **22**: 4009–4030.
- Woollard, A.A.D., and Moore, I.** (2008). The functions of Rab GTPases in plant membrane traffic. *Curr. Opin. Plant Biol.* **11**: 610–619.
- Zelazny, E., Santambrogio, M., Pourcher, M., Chambrier, P., Berne-Dedieu, A., Fobis-Loisy, I., Miège, C., Jaillais, Y., and Gaude, T.** (2013). Mechanisms governing the endosomal membrane recruitment of the core retromer in *Arabidopsis*. *J. Biol. Chem.* **288**: 8815–8825.
- Zhang, L., Zhang, H.Y., Liu, P., Hao, H.Q., Jin, J.B., and Lin, J.X.** (2011). *Arabidopsis* R-SNARE proteins VAMP721 and VAMP722 are required for cell plate formation. *PLoS ONE* **6**: e26129.
- Zhuang, X., Wang, H., Lam, S.K., Gao, C., Wang, X., Cai, Y., and Jiang, L.** (2013). A BAR-domain protein SH3P2, which binds to phosphatidylinositol 3-phosphate and ATG8, regulates autophagosome formation in *Arabidopsis*. *Plant Cell* **25**: 4596–4615.
- Zimmermann, P., Hirsch-Hoffmann, M., Hennig, L., and Gruissem, W.** (2004). GENEVESTIGATOR. *Arabidopsis* microarray database and analysis toolbox. *Plant Physiol.* **136**: 2621–2632.
- Zouhar, J., Rojo, E., and Bassham, D.C.** (2009). AtVPS45 is a positive regulator of the SYP41/SYP61/VTI12 SNARE complex involved in trafficking of vacuolar cargo. *Plant Physiol.* **149**: 1668–1678.

NOTE ADDED IN PROOF

Two articles related to this topic have recently been accepted for publication (Ebine et al., 2014; Singh et al., 2014).

Ebine, K., Inoue, T., Ito, J., Ito, E., Uemura, T., Goh, T., Abe, H., Sato, K., Nakano, A., and Ueda, T. (2014). Plant vacuolar trafficking occurs through distinctly regulated pathways. *Curr. Biol.*, in press.

Singh, M.K., Krüger, F., Beckmann, H., Brumm, S., Vermeer, J.E.M., Munnik, T., Mayer, U., Stierhof, Y.D., Grefen, C., Schumacher, K., and Jürgens, G. (2014). Protein delivery to vacuole requires SAND protein-dependent Rab GTPase conversion for MVB-vacuole fusion. *Curr. Biol.*, in press.